1. Introduction

We set out to discover what, if any, effect changing the mean square slope would have on the simulated radiance field above and below the ocean surface. We then studied how that effect changed with increase in depth. At each specific depth, we then compared the effects for wind speeds 5 m/s and 10 m/s, and solar zenith angle from 0 degrees and 30 degrees.

We used the simulation software Hydrolight 4.1, developed by Curtis D. Mobley, to study the effect of changing the mean square slope on the radiance field above and below the ocean surface. We started by using Elfouhaily's et al.[1] integral

$$\sigma^2 = \int_0^\infty k^2 s(k) dk \,. \tag{1}$$

to calculate the omnidirectional slope spectrum up to a large maximum wave number, for wind speed 5 m/s. We then began truncating the integral, removing the higher frequencies from the calculation. The process was repeated for wind speed 10 m/s. The table below shows the maximum wave number along with its corresponding wavelength and the mean square slopes, σ^2, calculated for winds of 5 and 10 m/s.

Wavelength λ [m]	Max Wave Number k [rad/m]	Mean Square Slope Wind = 5 m/s	Mean Square Slope Wind = 10 m/s
0.001	6283.185	0.0293	0.0575
0.040	157.080	0.0236	0.0370
0.200	31.416	0.0191	0.0262
0.800	7.854	0.0132	0.0207

Table 1 Integrated Mean Square Slope for wind speeds 5 m/s and 10 m/s up to the maximum wave number corresponding to each cut-off wavelength.

We then used the Cox and Munk[2] relation

$$\sigma^2 = 0.003 + 0.00512w \tag{2}$$

to calculate a corresponding wind speed, *w*, related to each mean square slope value. The table below shows the values that were used to run the Hydrolight software, although the program only allows wind speed values out to the hundredths place. We also ran the software at wind speed 0 m/s to serve as a comparison.

Mean Square Slope Wind = 5 m/s	Corresponding Wind Speed [m/s]	Mean Square Slope Wind = 10 m/s	Corresponding Wind Speed [m/s]
0.0293	5.138	0.0575	10.642
0.0236	4.015	0.0370	6.636
0.0191	3.149	0.0262	4.539
0.0132	1.993	0.0207	3.453

Table 2 Corresponding wind speed to each integrated mean square slope.

Originally, we ran the Hydrolight simulation at its default settings which divided the surfaces into 10 μ and 24 ϕ, where $\mu = \cos\theta$, θ is the polar angle and ϕ is the azimuth angle. The Hydrolight program generates a value at each point by calculating the average within the region surrounding that point. So, we decided that dividing the surface into more angles would create smaller regions and thereby give a better result. We generated the surface and phase function files for other angle configurations, including: 90 μ by 4 ϕ, 90 μ by 24 ϕ, and 20 μ by 24 ϕ. Taking accuracy and computation time into consideration, it was decided that the 20 μ by 24 ϕ setup was sufficient to answer the question.

Once the surface configuration was settled, we defined the characteristics of the atmosphere-ocean system that would be input into the Hydrolight software. A Petzold Phase Function was used to simulate the scattering phase function of the ocean. The other specified values, organized by input window, are given as follows:

The Inherent Optical Property Specification was ABCONST, which is a one-component, single wavelength, homogeneous water model using the total a and b. Where a and b are the total absorption coefficient and total scattering coefficient, and both are independent of depth.

The Total Absorption coefficient was 0.016 m^{-1}, as was the Total Scattering coefficient; thereby giving a total extinction coefficient of 0.032 m^{-1} with a single scattering albedo of 0.5. The Scattering Phase Function was Average Particle (Petzold) and the Wavelength was 530 nm.

The runs did not include bioluminescence, or inelastic scattering.

The wind speed was entered in m/s with the last significant digit in the hundredths place, and then the values were updated in the boxes defining other systems of units. We used a semi-empirical sky model, which is based on RADTRAN. We used zero degrees and 30 degrees to define the solar zenith angle. The cloud cover was always zero, giving a totally clear sky.

The atmospheric parameters that went along with the RADTRAN model were:
Sea-level pressure: 29.92 inches HG
24-hr Averaged Windspeed: our previous input
Average horizontal visibility: 15 km
Relative humidity: 80 %
Precipitable water content: 2.5 cm
Total Ozone: -99 Dobson units
Airmass type: 1 (to denote marine rather than continental)

The downwelling sky IRRADIANCE was specified by RADTRAN, which gave the direct (solar) and diffuse (sky) components of the irradiance. Both were calculated directly from the RADTRAN model. The ANGULAR PATTERN of

the sky radiance distribution was obtained from a subroutine, in the maincode directory, named hcnrad.

We used an infinitely deep water column to avoid any interfering radiance reflected up from the bottom, and we took data at specific optical depths. By default, Hydrolight places a detector just above the ocean surface, to define the input, and just below the ocean surface. We also placed detectors at optical depths 1, 2, 5, and 10, corresponding to actual depths of 31.25, 62.50, 156.25, and 312.5 meters.

2. Wind Speed 0 m/s

To serve as a basis of comparison, we ran the Hydrolight software for wind speed 0 m/s at each optical depth. All of the figures presented here will show data in the principal plane, only. The principal plane is defined by the azimuth position of the sun, set to ϕ =180 degrees, and the azimuth position opposite to the sun, at ϕ = 0 degrees. Figure 1 shows a diagram of the solar zenith angle location as well as the detector polar angles used to generate all of our graphs.

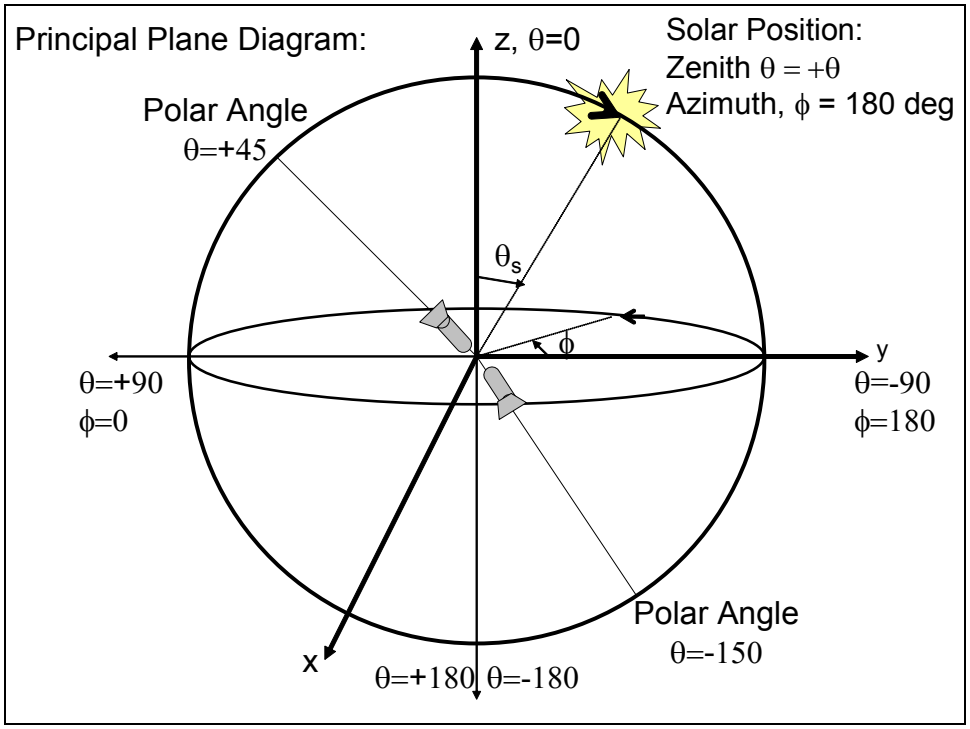

Figure 1 Diagram of solar and detector positions in the Principal Plane. The polar angles defined in this diagram were used to generate all of the graphs presented here.

Figure 2 and Figure 3 show the radiance versus polar angle plot for each detector with a solar zenith angle of 0 degrees and 30 degrees. The +ε and -ε curves refer to the radiance directly above and below the sea surface, respectively.

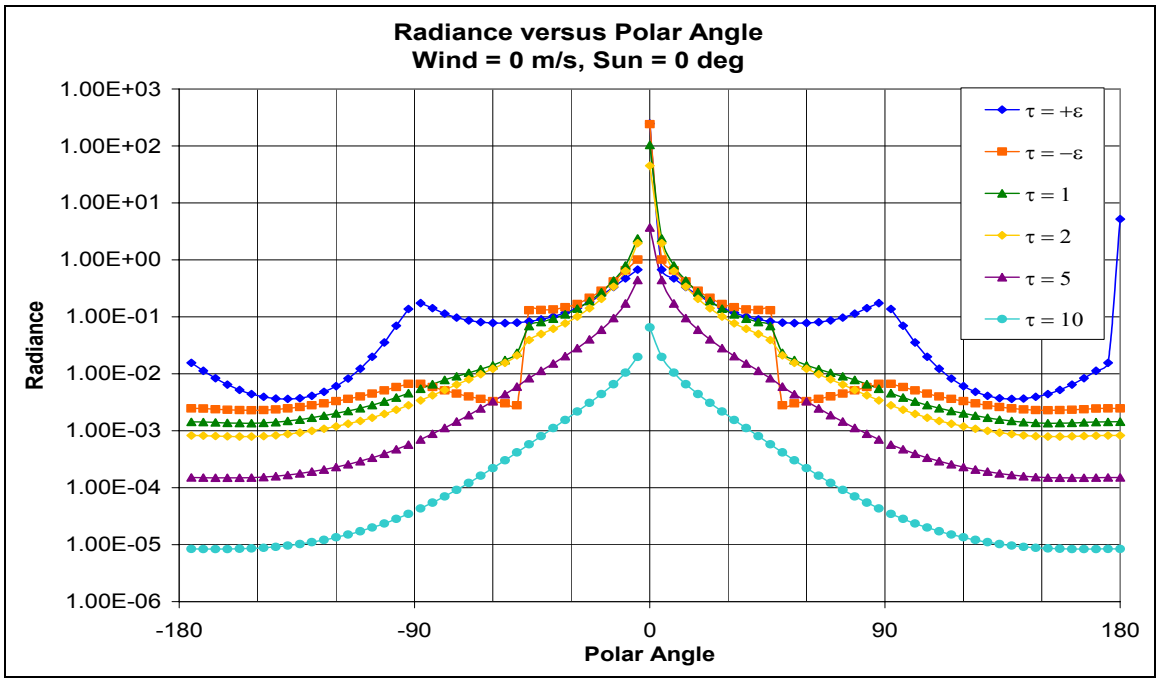

Figure 2 Logarithmic Radiance versus Polar Angle graph for detectors just above and below the sea surface and at optical depths 1, 2, 5 and 10. Wind speed 0 m/s and solar zenith angle 0 degrees.

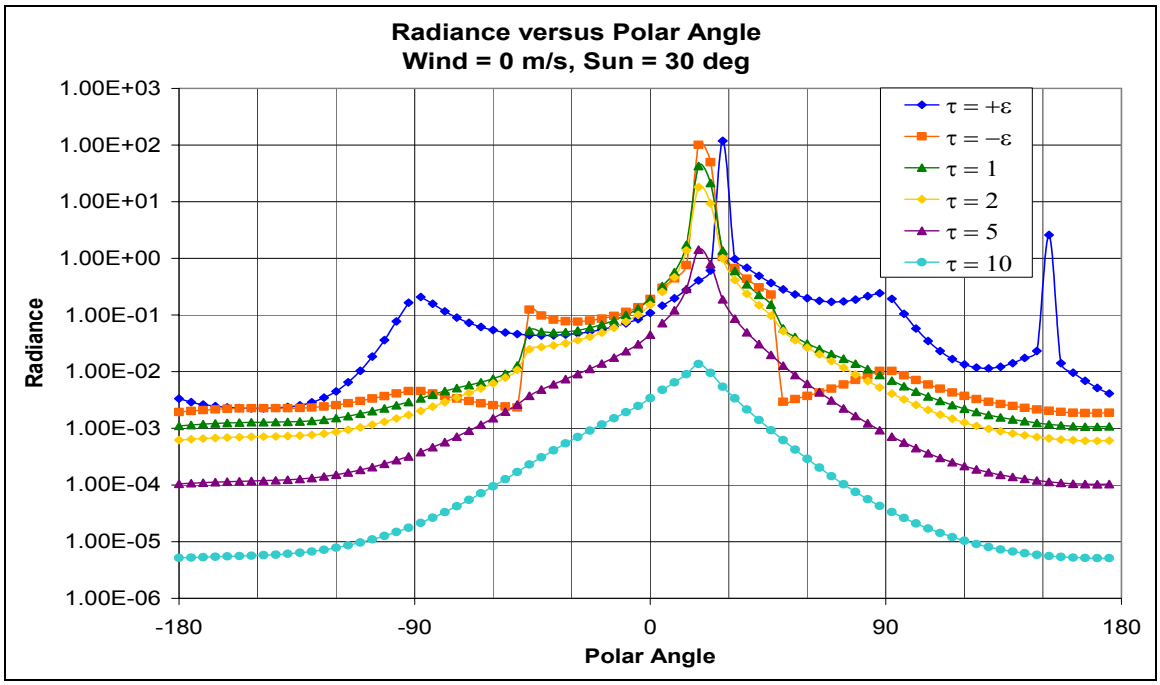

Figure 3 Logarithmic Radiance versus Polar Angle graph for detectors just above and below the sea surface and at optical depths 1, 2, 5 and 10. Wind speed is 0 m/s, solar zenith angle is 30 degrees.

Using the wind speed 0 m/s cases we were able to check the computational accuracy of the code. We compared the radiance above the surface to the radiance at the refracted

angle below the surface to be sure that the n^2 factor was maintained[3]. Outside of the direct beam, we were able to recreate the ratio with reasonable accuracy, since the program calculates the radiance at a given angle by averaging the values in the surrounding surface element.

We were also able to compare the radiance values to the experimentally shown[4] drop-off with depth. Both of the checks were satisfied by the code and we were then able to perform the higher wind speed simulations.

3. Wind Speed 5 m/s

In order to study the effect of changing the mean square slope on the radiance field above and below the ocean surface, we compared the radiance curves for different corresponding wind speed at each optical depth. We considered the data from the highest maximum wave number value, and shortest cut-off wavelength, as our value for the non-truncated spectrum, since it included the most frequencies in the integral. We then calculated the percent difference between the value for the non-truncated spectrum and the data at each other corresponding wind speed. We began with a solar zenith angle of zero degrees.

Figure 4 shows the radiance versus polar angle dependence, at each corresponding wind speed, above the sea surface. The curve for wind speed 0 m/s is also included as a point of comparison. Figure 5 shows the percent difference to the value for the non-truncated spectrum, the $\lambda = 0.001$ case, for each corresponding wind speed, above the sea surface. The breaks between points in all of the included figures are artifacts, and the curves are truly continuous.

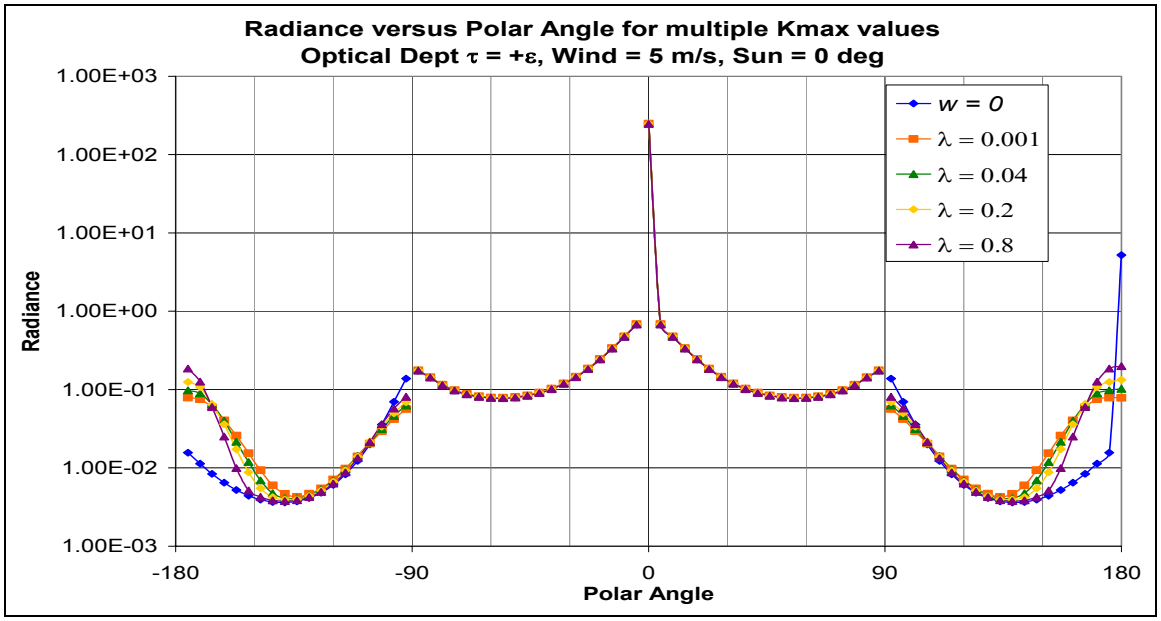

Figure 4 Logarithmic Radiance versus Polar Angle graph for detectors just above the sea surface at multiple K_{max} values corresponding to cut-off wavelengths 0.001, 0.04, 0.2, and 0.8 meters. Solar zenith angle 0 degrees. Wind speed, *w*, of 0 m/s is included as a comparison.

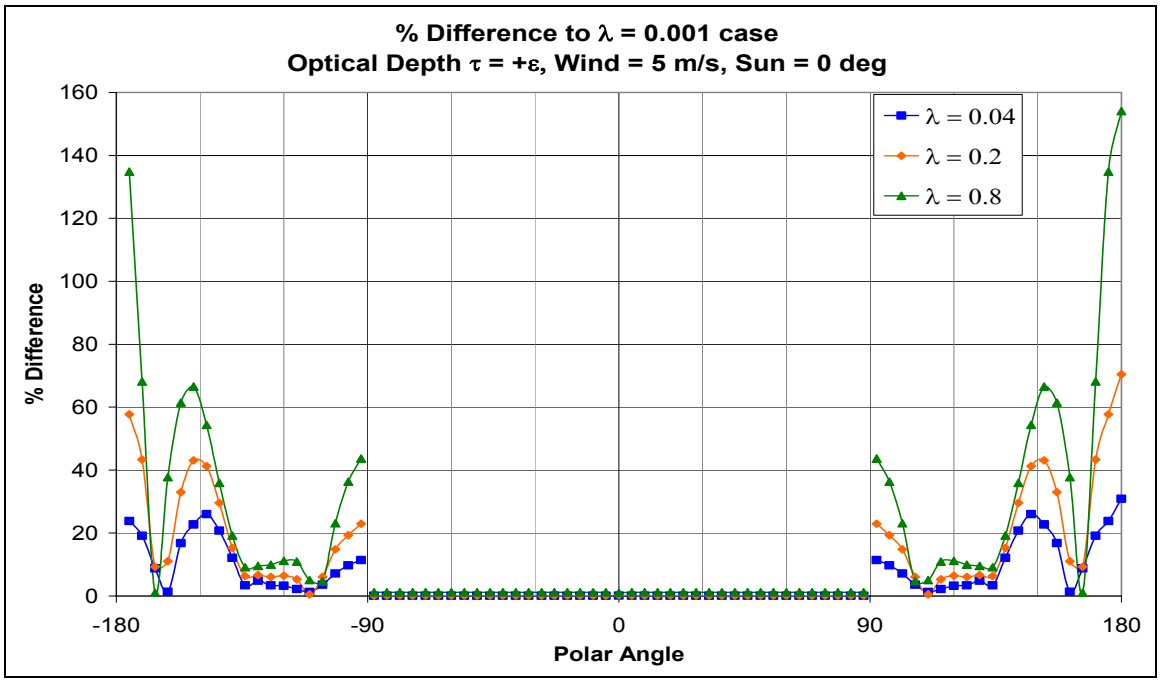

Figure 5 Percent Difference Between Longer Cut-off Wavelengths and the λ = 0.001 Case versus Polar Angle graph for detectors just above the sea surface.

From polar angles -90 degrees to 90 degrees there is no difference in radiance just above the sea surface with changing wind speed. This makes sense because polar angle zero degrees corresponds to downwelling radiation (the detector is oriented directly upward) and Hydrolight does not consider the interaction between the ocean and the atmosphere. The downward detector orientations show greater percent difference with each longer cut-off wavelength, or smaller maximum wave number. In these plots, as well as all plots with a solar zenith angle of zero degrees, there is perfect mirror symmetry about polar angle zero, due to the azimuthal independence of the radiance.

Below the sea surface the radiance versus polar angle graphs show maximum difference between the curves when the detector is oriented upward. Figure 6 and Figure 7 show the radiance and percent difference relationships just below the sea surface, respectively.

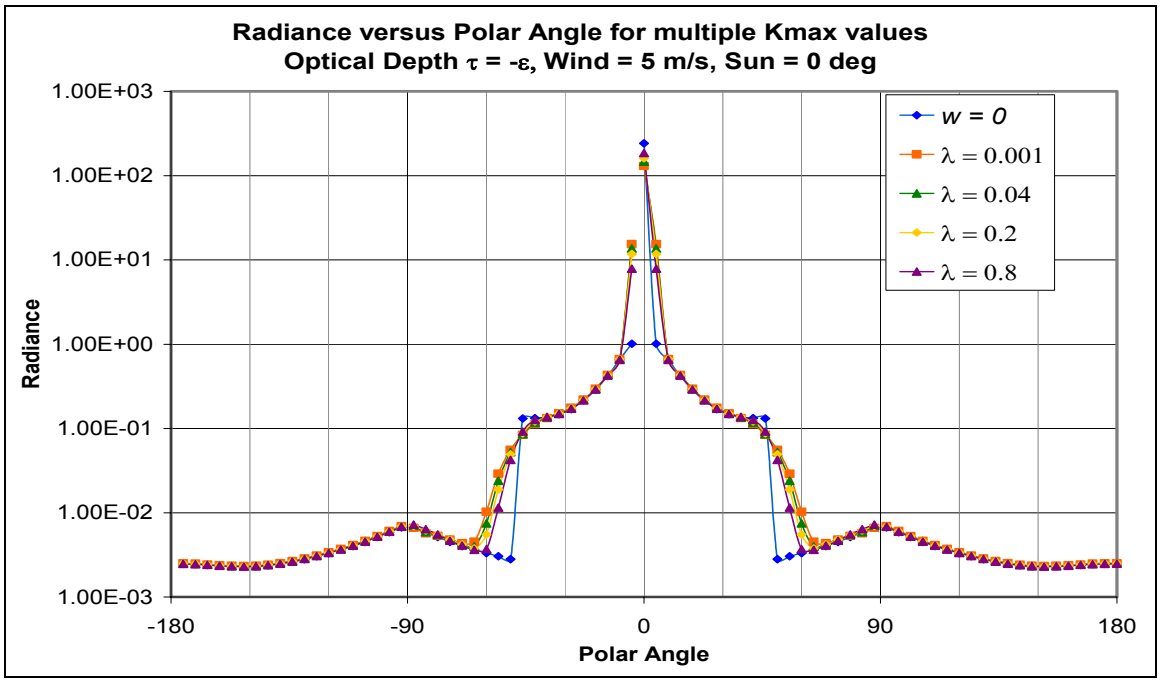

Figure 6 Logarithmic Radiance versus Polar Angle graph for detectors just below the sea surface at multiple K_{max} values corresponding to cut=off wavelengths 0.001, 0.04, 0.2, and 0.8 meters. Solar zenith angle 0 degrees. Wind speed, *w*, of 0 m/s is included as a comparison.

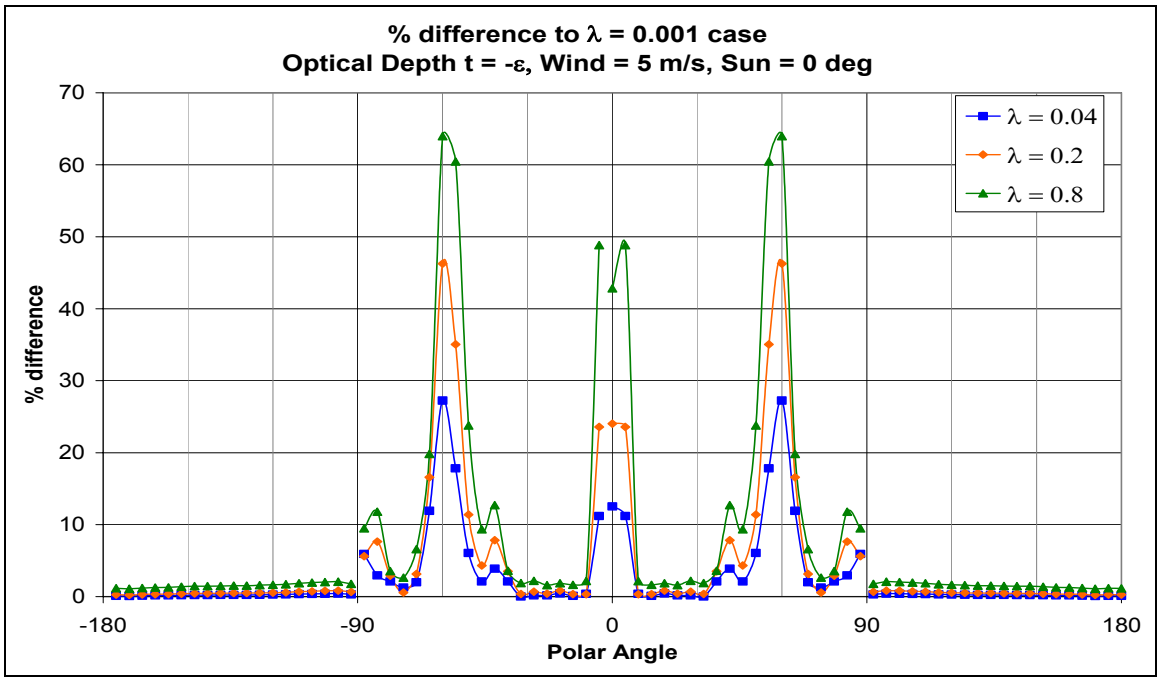

Figure 7 Percent Difference Between Longer Cut-off Wavelengths and the λ = 0.001 Case versus Polar Angle graph for detectors just below the sea surface.

The maximum percent difference is found in the diffuse region around -48 degrees and 48 degrees, which is the critical angle for a flat sea surface. There is also a significant difference in the solar beam, located at polar angle zero degrees. As with the detectors above the sea surface, the data for longest cut-off wavelength also shows the largest percent difference to the value for the non-truncated spectrum.

Those relationships continue as detectors are placed at increasing depth. Figure 8 and Figure 9 show the radiance and percent difference relations at optical depth one, which is a true depth of 31.25 meters.

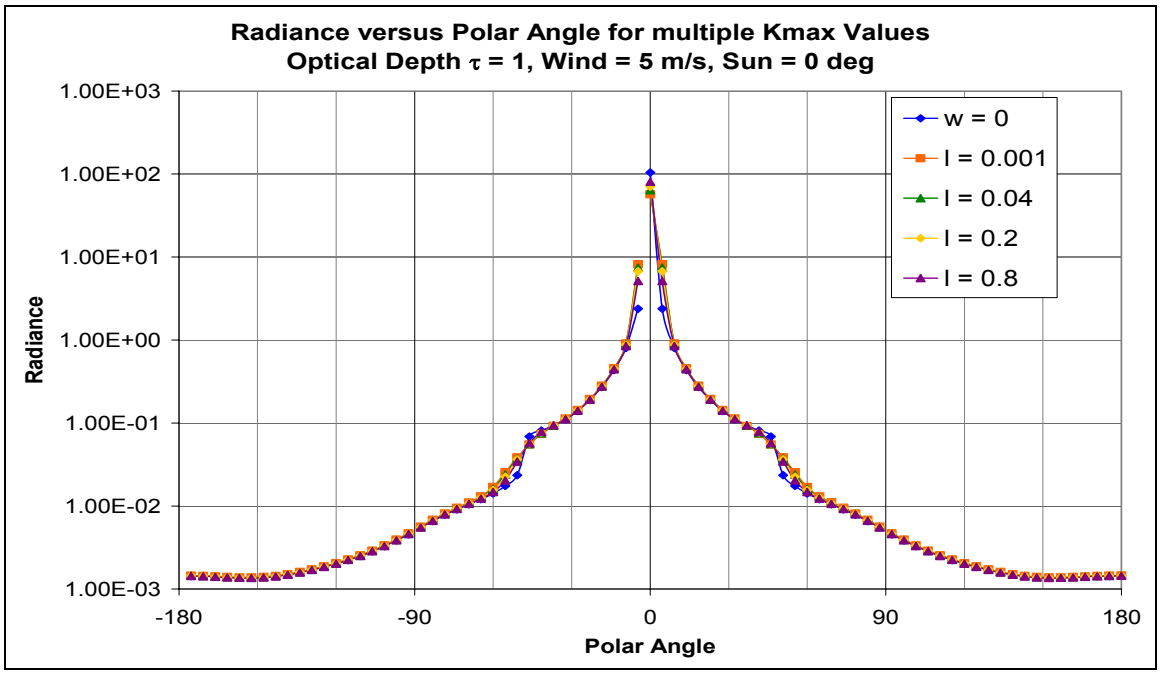

Figure 8 Logarithmic Radiance versus Polar Angle graph for detectors at optical depth 1, below the sea surface, at multiple K_{max} values corresponding to cut-off wavelengths 0.001, 0.04, 0.2, and 0.8 meters. Solar zenith angle 0 degrees. Wind speed, *w*, of 0 m/s is included as a comparison.

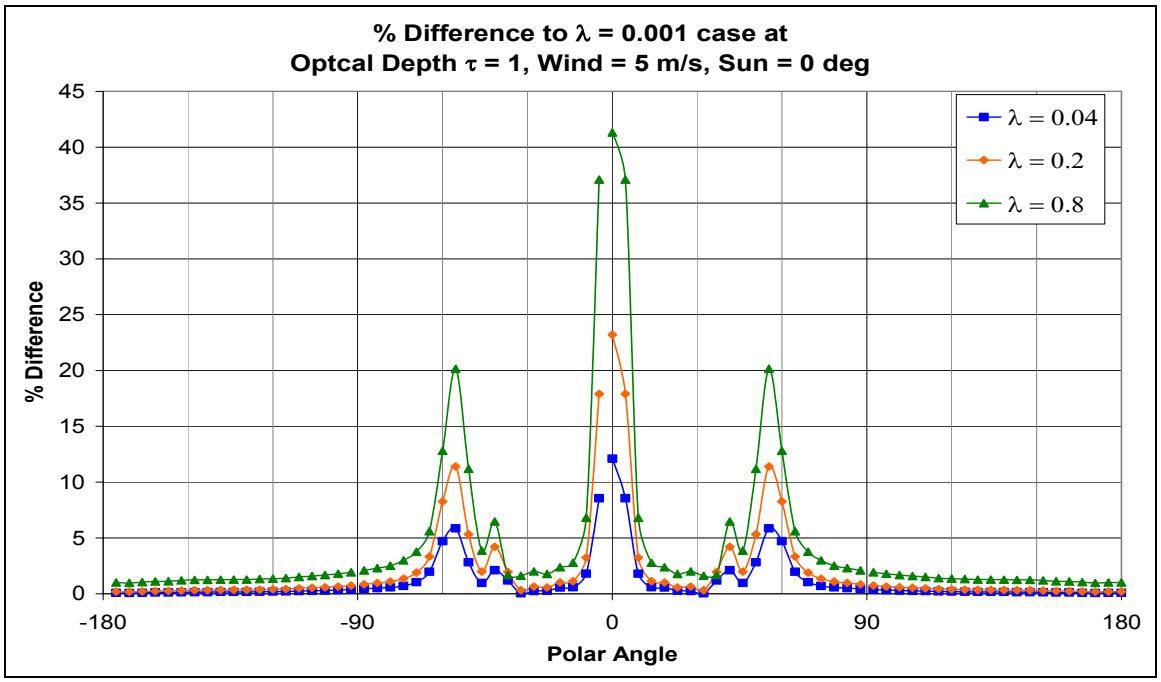

Figure 9 Percent Difference Between Longer Cut-off Wavelengths and the λ = 0.001 Case versus Polar Angle graph for detectors at optical depth 1 below the sea surface.

Contrary to the detectors just below the sea surface, the maximum percent difference is in the direction of the solar beam, with a smaller difference in the diffuse region around -48 degrees and 48 degrees. Also, with this greater depth, the peak percent differences are smaller. This trend of shape will continue at greater depths.

With increasing depth, the changes in corresponding wind speed, and therefore maximum wave number and cut-off wavelength, will have less and less effect on the radiance curves. Figure 10 and Figure 11 show the radiance and percent difference relations at optical depth two, which is a true depth of 62.50 meters.

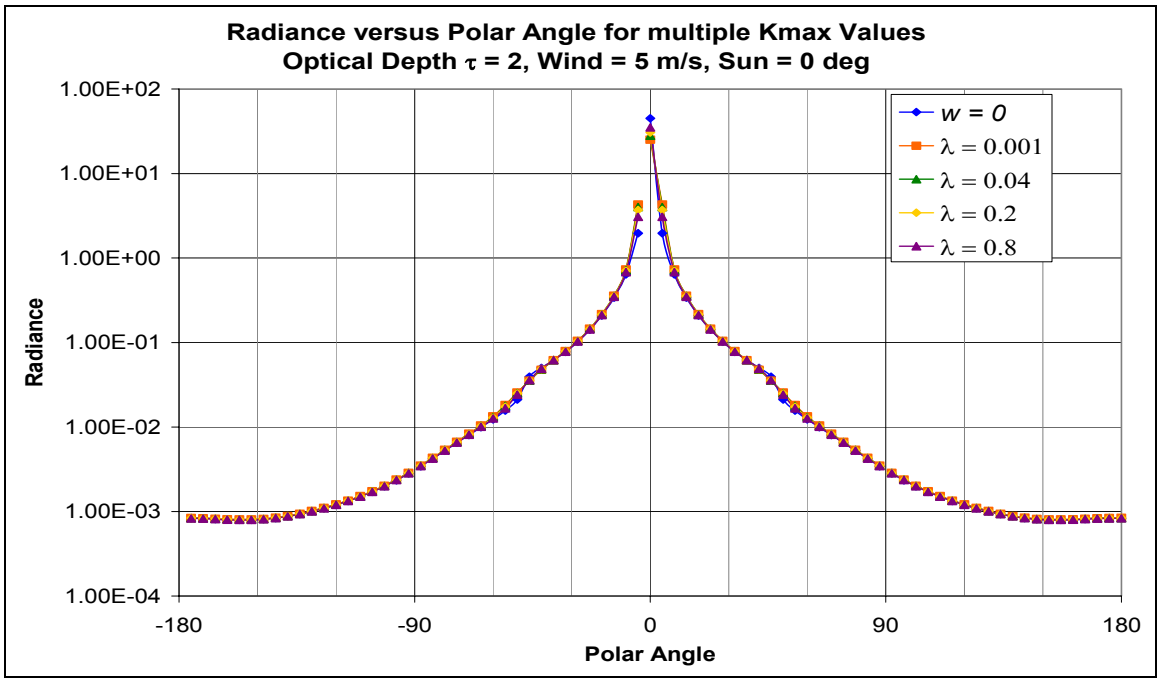

Figure 10 Logarithmic Radiance versus Polar Angle graph for detectors at optical depth 2, below the sea surface, at multiple K_{max} values corresponding to cut-off wavelengths 0.001, 0.04, 0.2, and 0.8 meters. Solar zenith angle 0 degrees. Wind speed, *w*, of 0 m/s is included as a comparison.

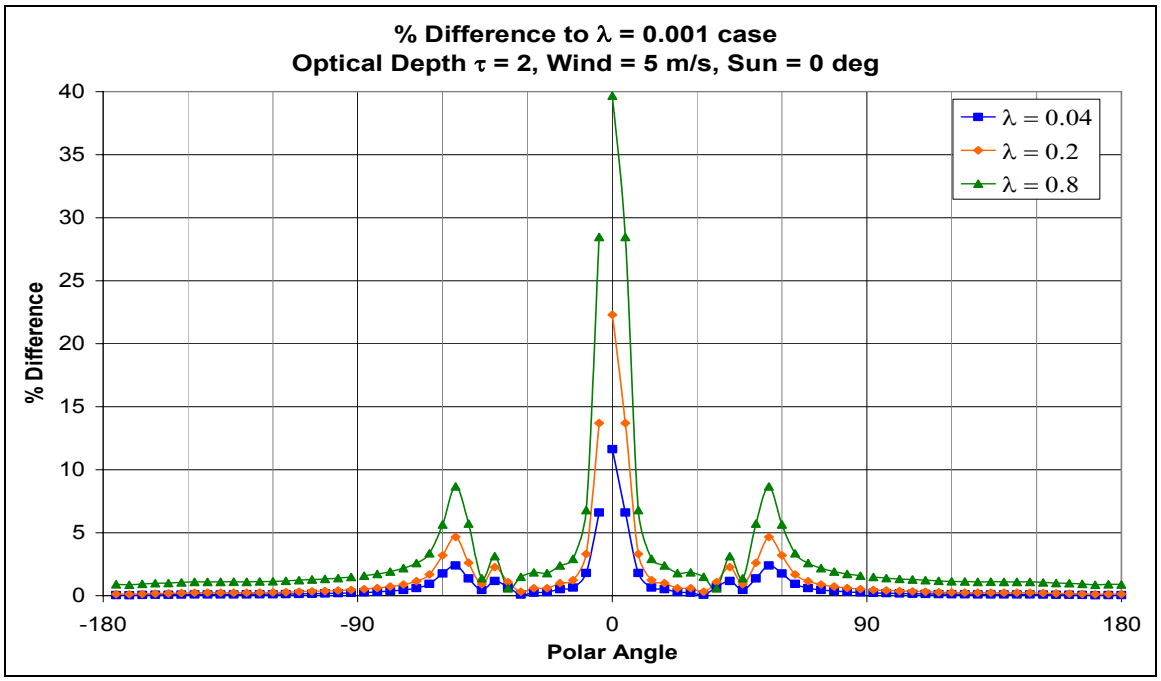

Figure 11 Percent Difference Between Longer Cut-off Wavelengths and the λ = 0.001 Case versus Polar Angle graph for detectors at optical depth 2 below the sea surface.

Figure 12 and Figure 13 show the radiance and percent difference relations at optical depth five, which is a true depth of 156.25 meters.

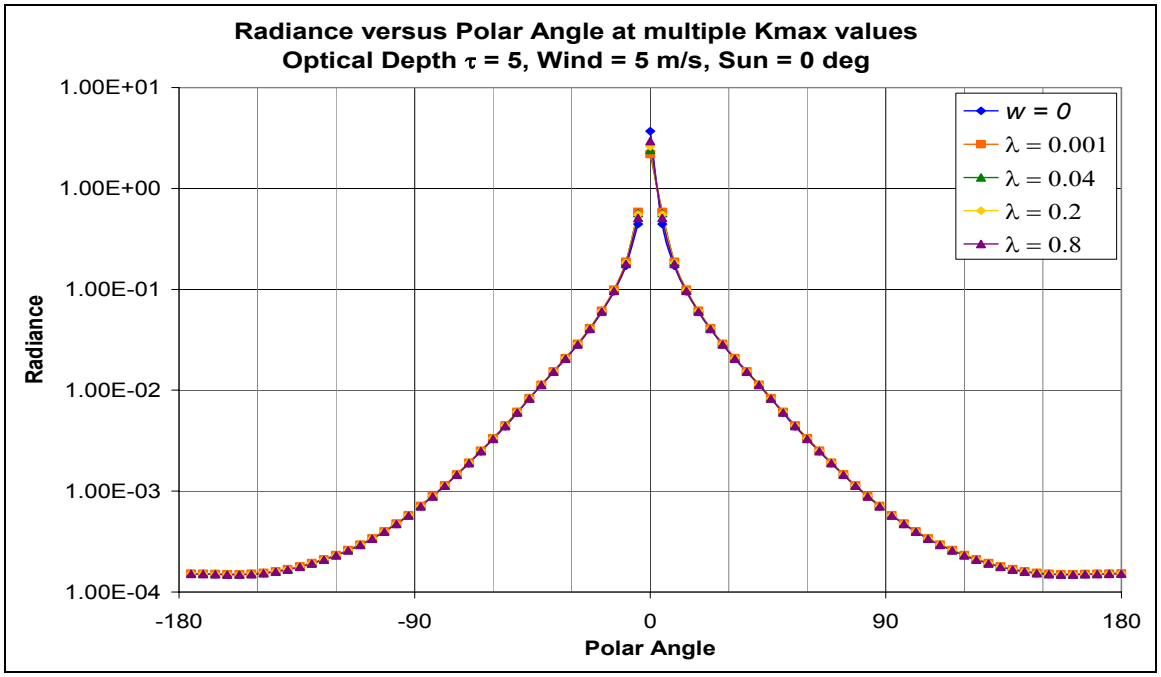

Figure 12 Logarithmic Radiance versus Polar Angle graph for detectors at optical depth 5, below the sea surface, at multiple K_{max} values corresponding to cut-off wavelengths 0.001, 0.04, 0.2, and 0.8 meters. Solar zenith angle 0 degrees. Wind speed, *w*, of 0 m/s is included as a comparison.

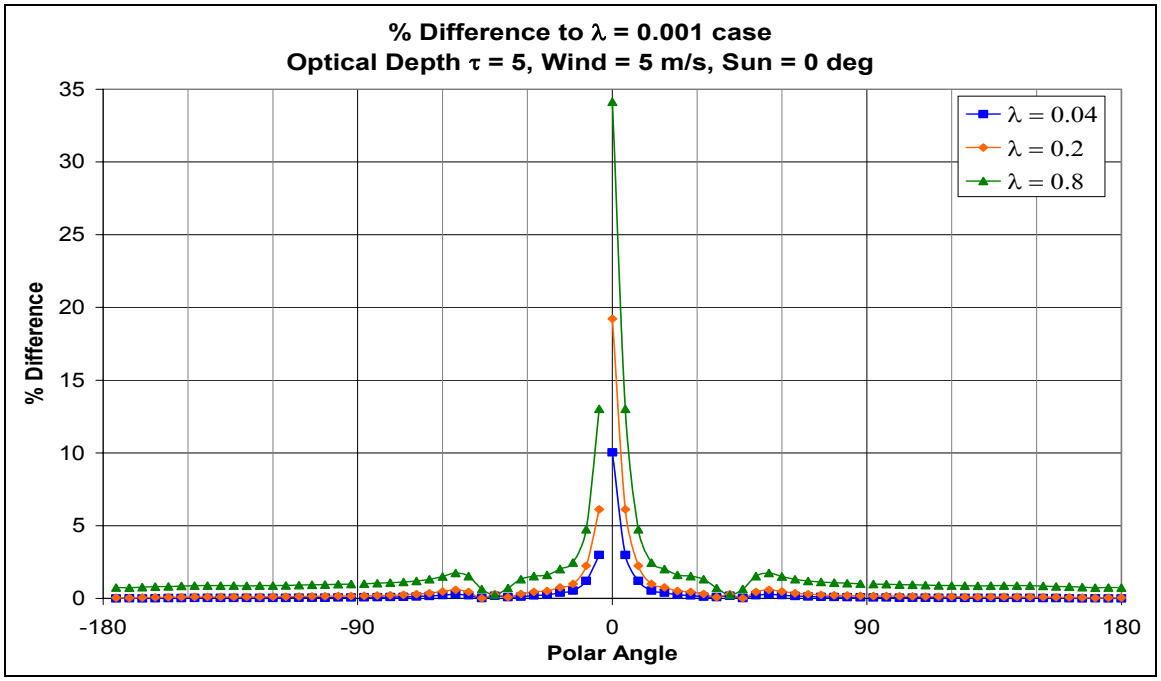

Figure 13 Percent Difference Between Longer Cut-off Wavelengths and the λ = 0.001 Case versus Polar Angle graph for detectors at optical depth 5 below the sea surface.

With these last two locations, at optical depths five and ten, the peak percent difference in the diffuse region has decreased such that it is nearly nonexistent. However, the maximum peak in the solar beam remains strong. Figure 14 and Figure 15 show the radiance and percent difference relations at optical depth ten, which is a true depth of 312.50 meters.

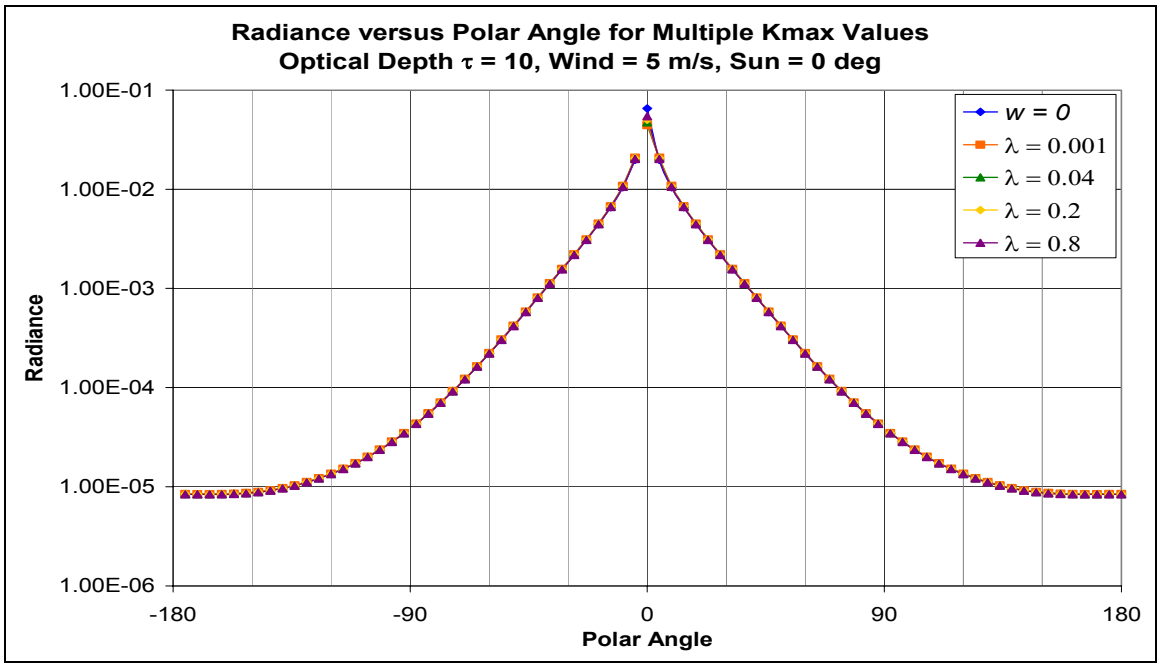

Figure 14 Logarithmic Radiance versus Polar Angle graph for detectors at optical depth 10, below the sea surface, at multiple K_{max} values corresponding to cut-off wavelengths 0.001, 0.04, 0.2, and 0.8 meters. Solar zenith angle 0 degrees. Wind speed, *w*, of 0 m/s is included as a comparison.

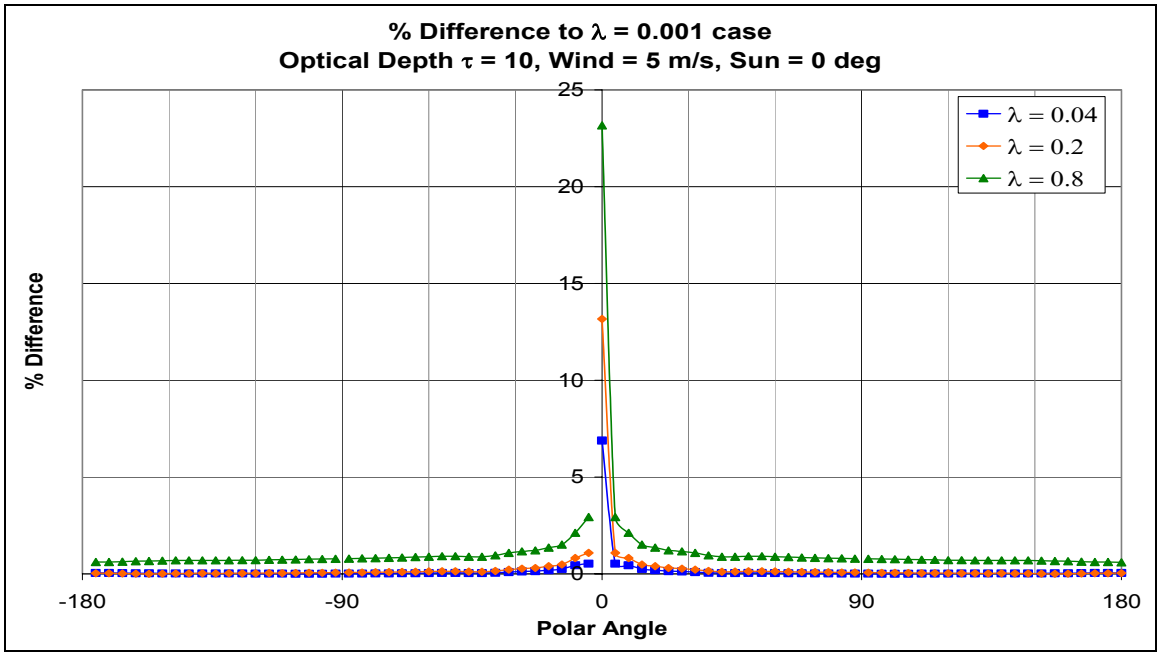

Figure 15 Percent Difference Between Longer Cut-off Wavelengths and the λ = 0.001 Case versus Polar Angle graph for detectors at optical depth 10 below the sea surface.

In order to determine if these differences are also found in more complex situations, we ran all of the same corresponding wind speeds and depths with solar zenith angle 30 degrees.

We found that, although the angular location of the solar beam had changed, the trends observed in the solar zenith angle 0 degrees case were maintained. Figure 16 and Figure 17 show the radiance and percent difference relationships just above the sea surface.

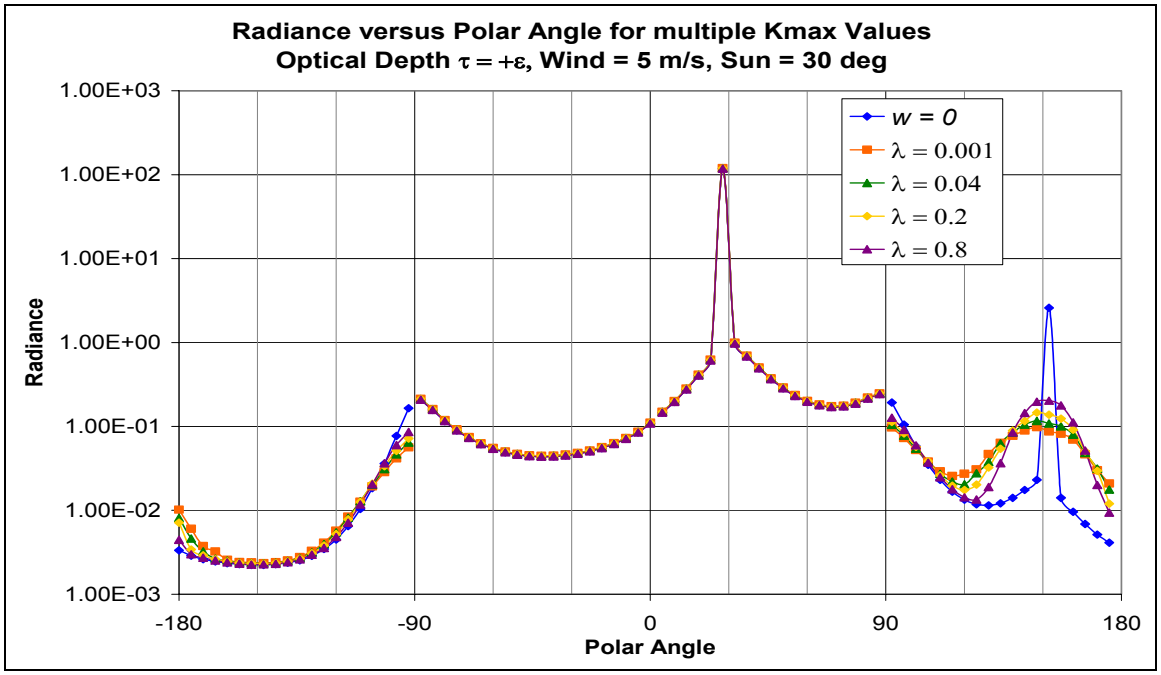

Figure 16 Logarithmic Radiance versus Polar Angle graph for detectors just above the sea surface, at multiple K_{max} values corresponding to cut-off wavelengths 0.001, 0.04, 0.2, and 0.8 meters. Solar zenith angle 30 degrees. Wind speed, *w*, of 0 m/s is included as a comparison.

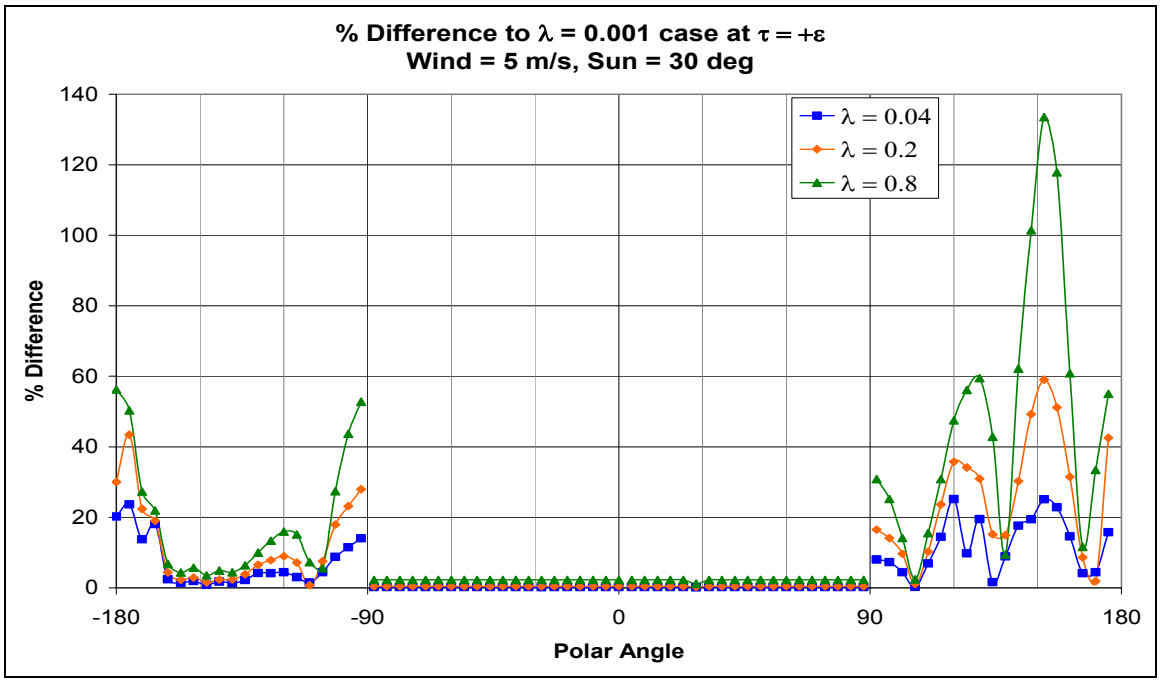

Figure 17 Percent Difference Between Longer Cut-off Wavelengths and the λ = 0.001 Case versus Polar Angle graph for detectors just above the sea surface.

As with the solar zenith angle 0 degrees case, the peak percent difference is at the angular location of reflected sunlight. Figure 18 and Figure 19 show the radiance and percent difference relationships just below the surface, for solar zenith angle 30 degrees.

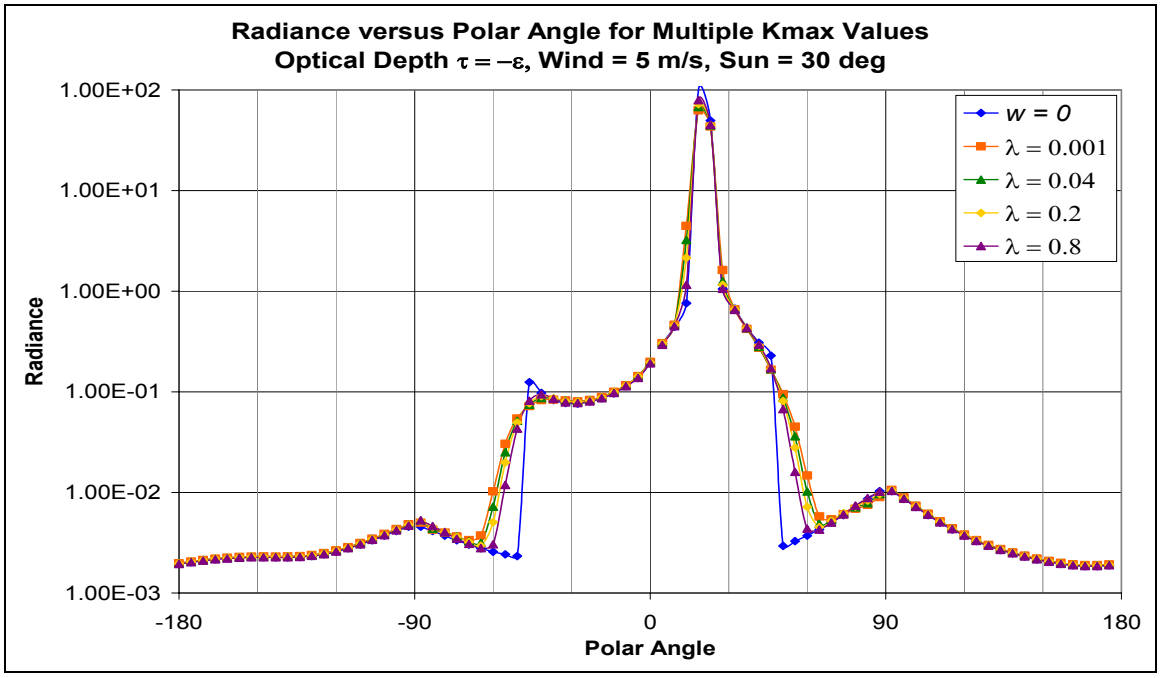

Figure 18 Logarithmic Radiance versus Polar Angle graph for detectors just below the sea surface, and multiple K_{max} values corresponding to cut-off wavelengths 0.001, 0.04, 0.2, and 0.8 meters. Solar zenith angle 30 degrees. Wind speed, *w*, of 0 m/s is included as a comparison.

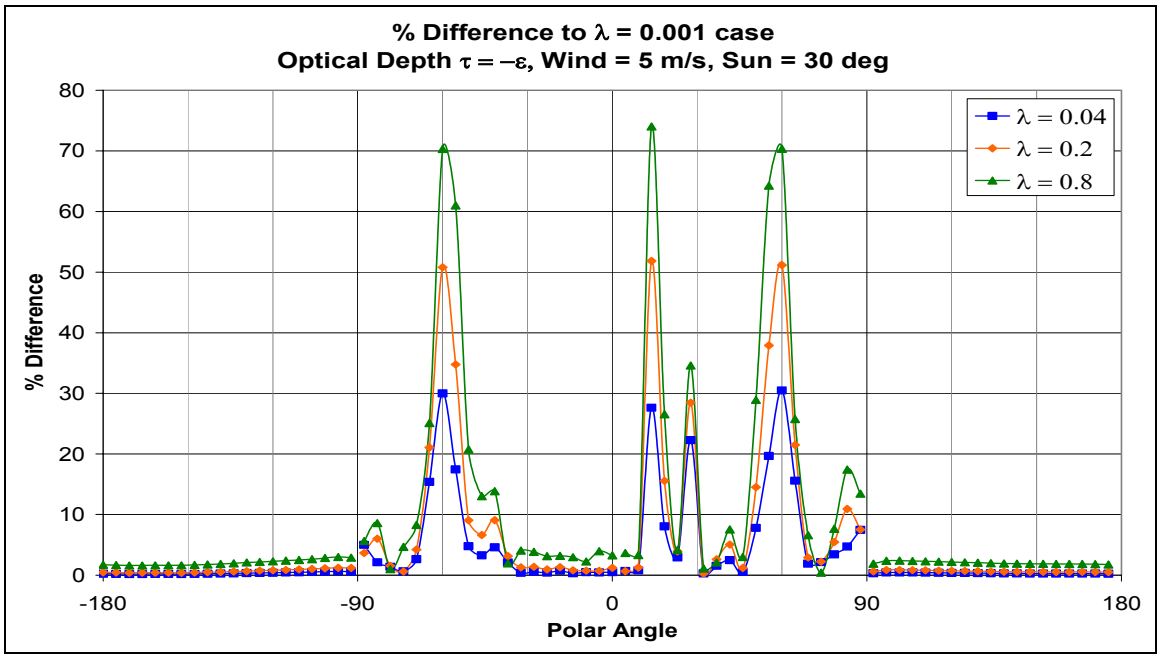

Figure 19 Percent Difference Between Longer Cut-off Wavelengths and the λ = 0.001 Case versus Polar Angle graph for detectors just below the sea surface.

As in the Solar Zenith Angle 0 degrees case, the peak percent differences are located in the diffuse region as well as in the refracted solar beam. These trends continue throughout the multiple depths. Figure 20 and Figure 21 show the radiance and percent difference relationships at optical depth 1 below surface, for solar zenith angle 30 degrees.

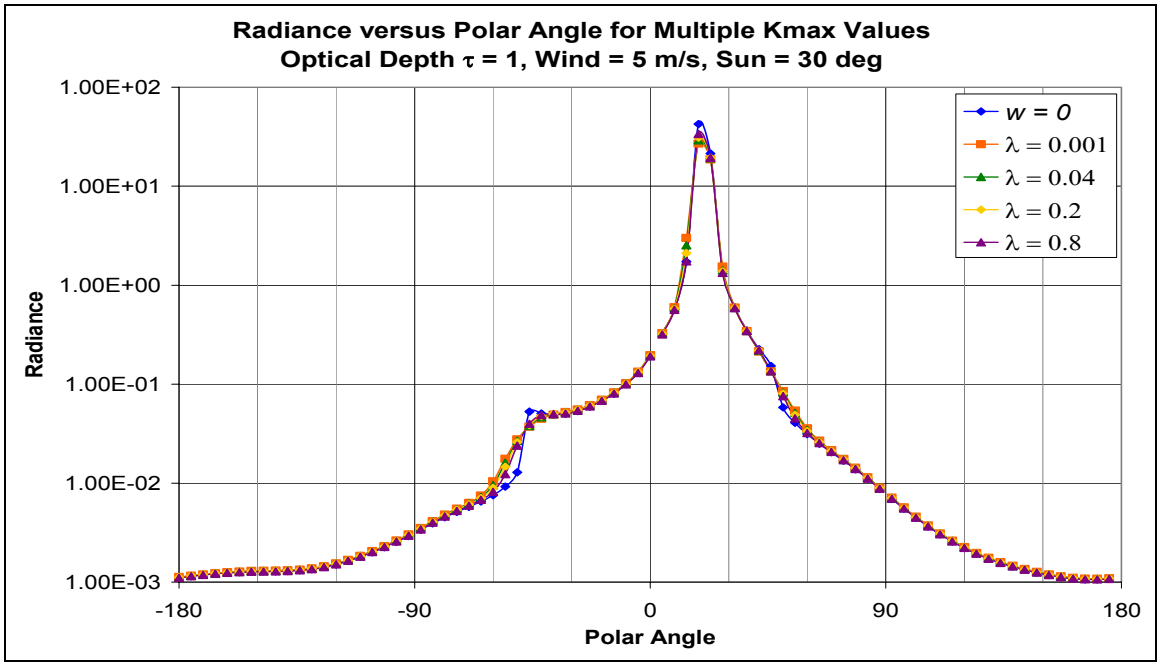

Figure 20 Logarithmic Radiance versus Polar Angle graph for detectors at optical depth 1 below the sea surface, and multiple K_{max} values corresponding to cut-off wavelengths 0.001, 0.04, 0.2, and 0.8 meters. Solar zenith angle 30 degrees. Wind speed, *w*, of 0 m/s is included as a comparison.

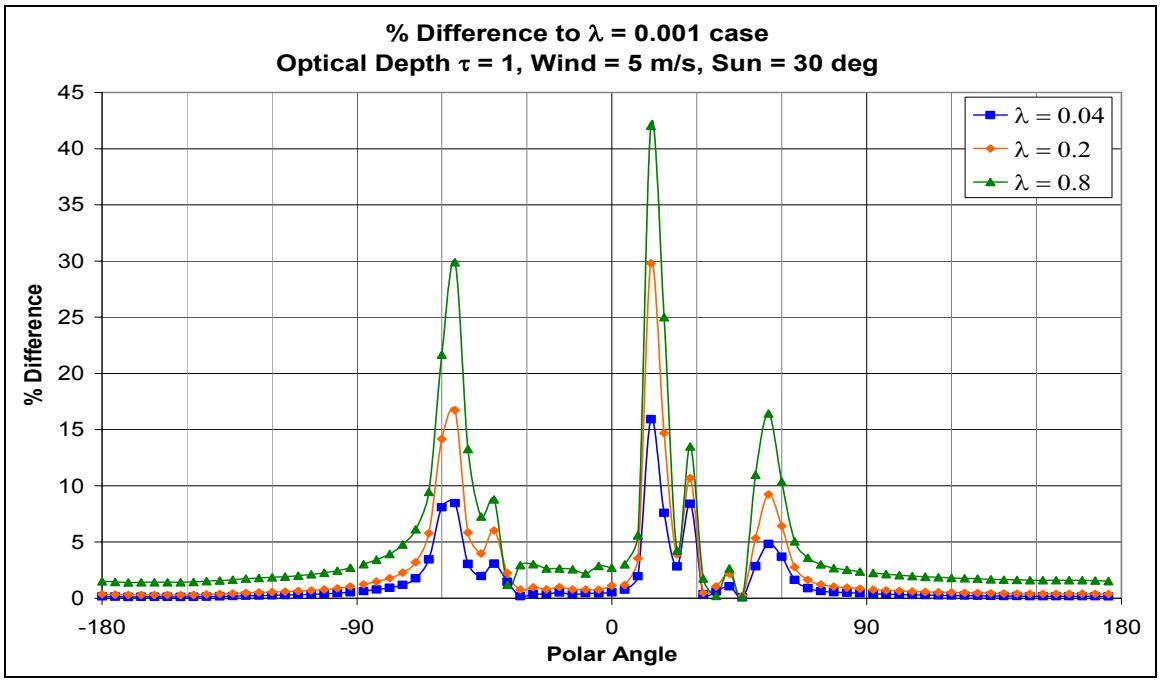

Figure 21 Percent Difference Between Longer Cut-off Wavelengths and the λ = 0.001 Case versus Polar Angle graph for detectors at optical depth 1 below the sea surface.

Unlike the solar zenith angle 0 degrees case, and the case with detectors just below the surface with solar zenith angle 30 degrees, the optical depth one data does not show equal peak percent differences in the diffuse region, around 48 degrees and -48 degrees.

In the subsequent depths, the peak percent differences, in the diffuse region, continue to be unequal. Figure 22 and Figure 23 show the radiance and percent difference relationships at optical depth 2 below surface, for solar zenith angle 30 degrees.

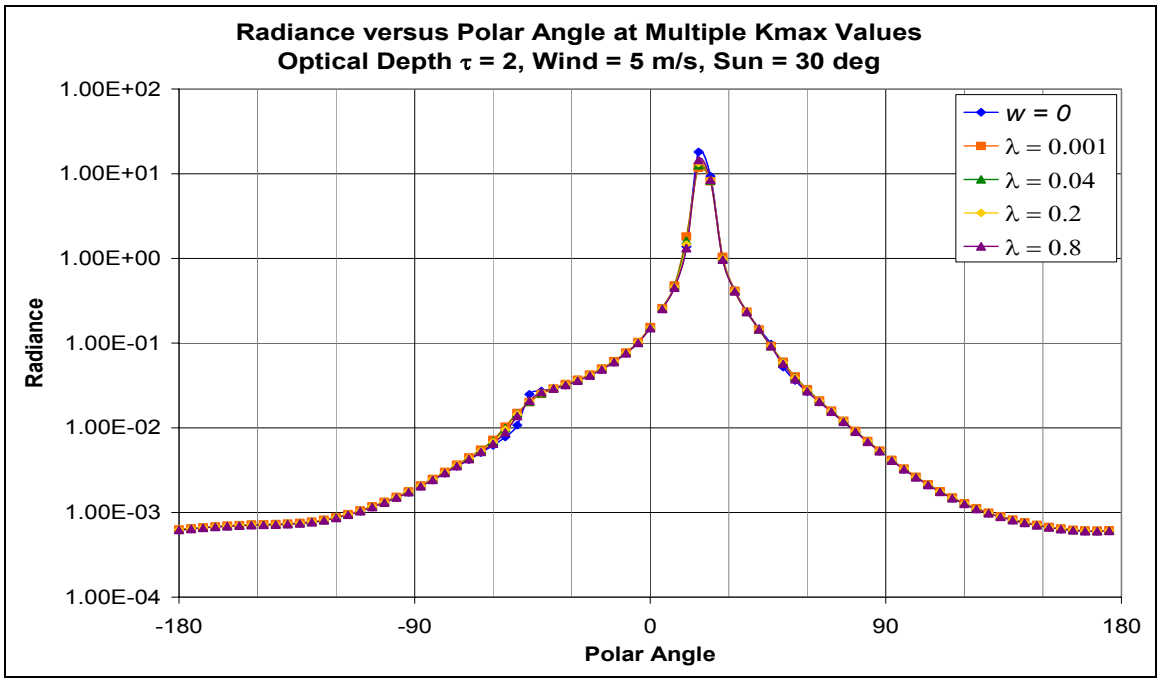

Figure 22 Logarithmic Radiance versus Polar Angle graph for detectors at optical depth 2 below the sea surface, and multiple K_{max} values corresponding to cut-off wavelengths 0.001, 0.04, 0.2, and 0.8 meters. Solar zenith angle 30 degrees. Wind speed, *w*, of 0 m/s is included as a comparison.

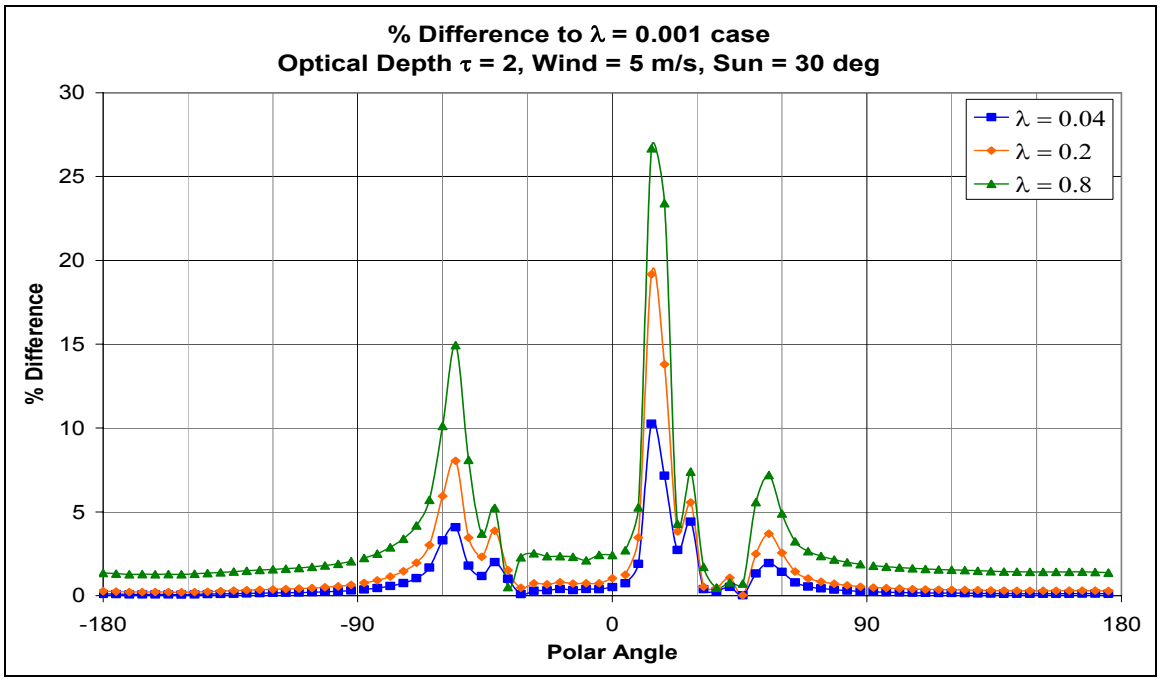

Figure 23 Percent Difference Between Longer Cut-off Wavelengths and the λ = 0.001 Case versus Polar Angle graph for detectors at optical depth 2 below the sea surface.

Figure 24 and Figure 25 show the radiance and percent difference relationships at optical depth 5 below surface, for solar zenith angle 30 degrees.

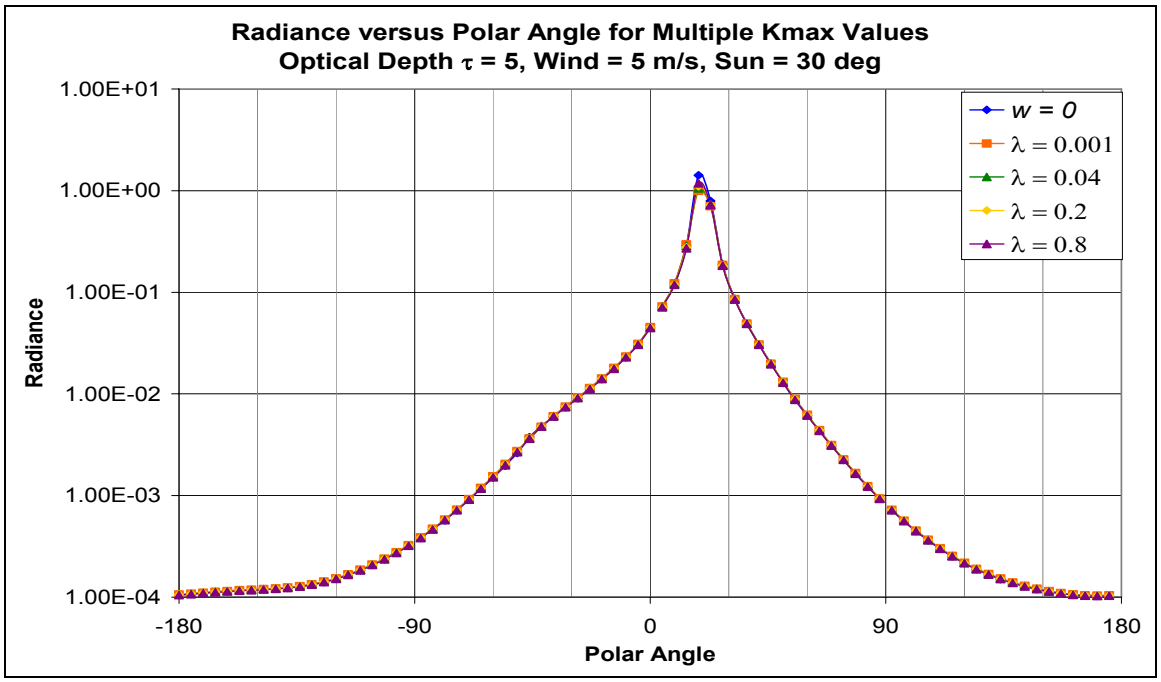

Figure 24 Logarithmic Radiance versus Polar Angle graph for detectors at optical depth 5 below the sea surface, and multiple K_{max} values corresponding to cut-off wavelengths 0.001, 0.04, 0.2, and 0.8 meters. Solar zenith angle 30 degrees. Wind speed, *w*, of 0 m/s is included as a comparison.

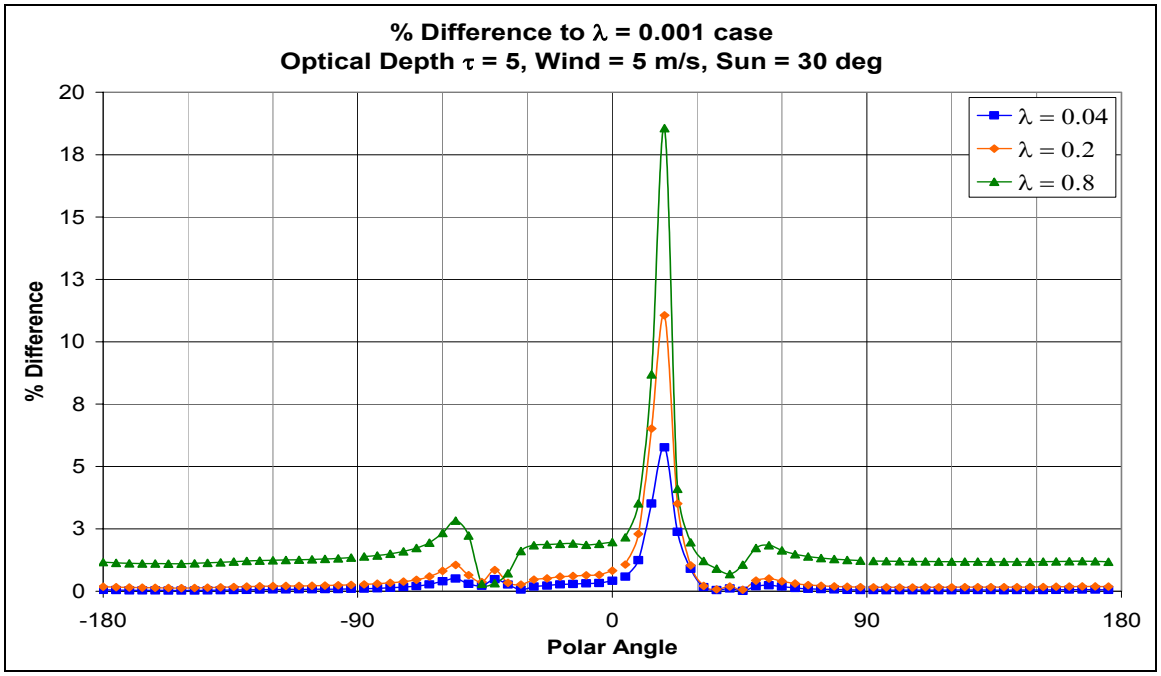

Figure 25 Percent Difference Between Longer Cut-off Wavelengths and the λ = 0.001 Case versus Polar Angle graph for detectors at optical depth 5 below the sea surface.

Figure 26 and Figure 27 show the radiance and percent difference relationships at optical depth 10 below surface, for solar zenith angle 30 degrees.

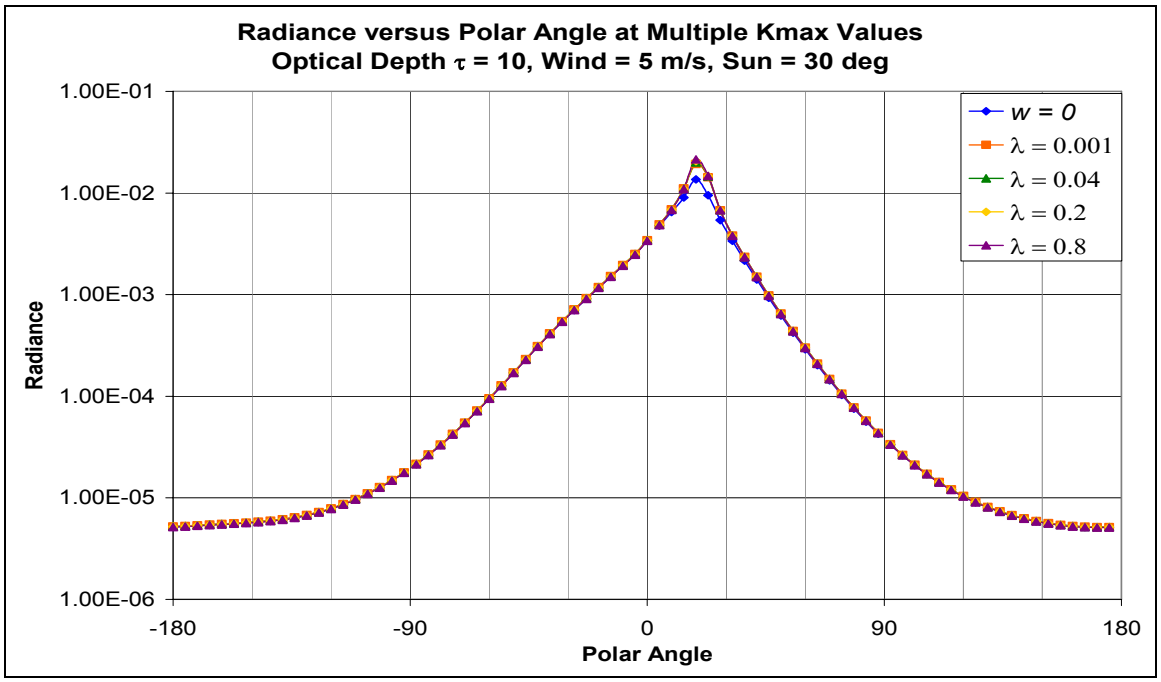

Figure 26 Logarithmic Radiance versus Polar Angle graph for detectors at optical depth 10 below the sea surface, and multiple K_{max} values corresponding to cut-off wavelengths 0.001, 0.04, 0.2, and 0.8 meters. Solar zenith angle 30 degrees. Wind speed, *w*, of 0 m/s is included as a comparison.

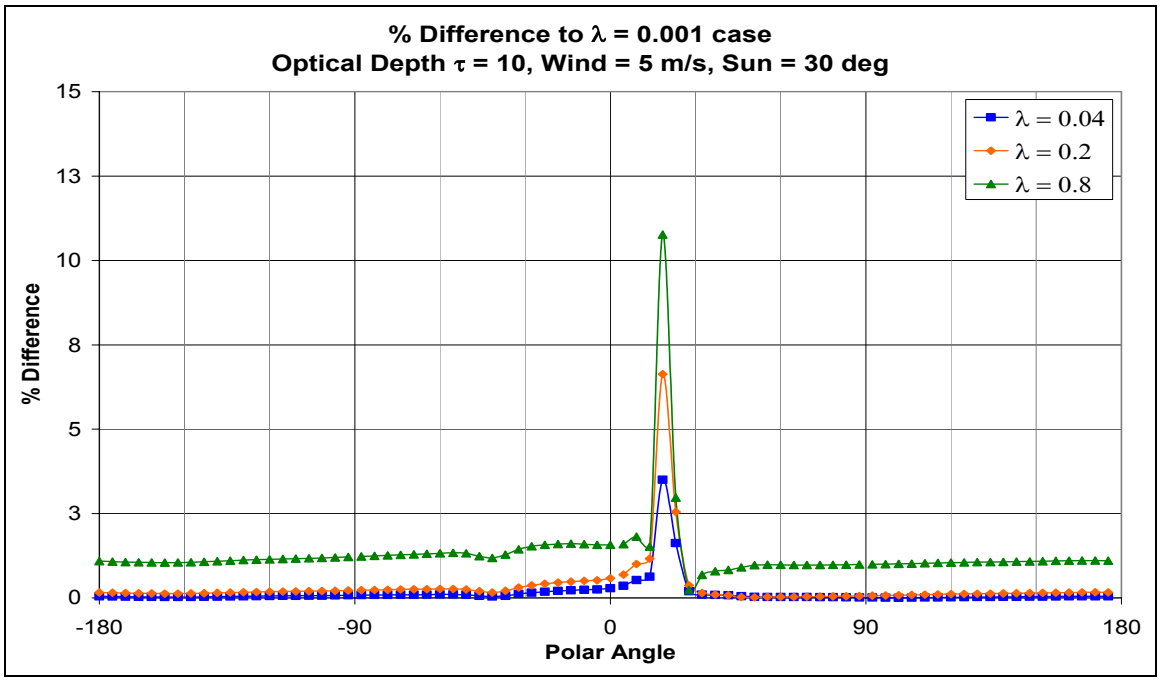

Figure 27 Percent Difference Between Longer Cut-off Wavelengths and the λ = 0.001 Case versus Polar Angle graph for detectors at optical depth 10 below the sea surface.

Although the location of the peak percent difference changed with solar zenith angle, both situations show a large percent difference in radiance in the diffuse and beam

regions. Removing the higher frequencies, shorter wavelengths, from the mean square slope calculation, by integrating to a smaller maximum wave number, has a definite effect on the outcome of the radiance simulation. This effect is less at greater depths.

4. Wind Speed 10 m/s

As with the wind speed 5 m/s simulation, we calculated the corresponding wind speed for mean square slope integrated to particular maximum wave number values. The trends observed in the wind speed 5 m/s cases were also present in the wind speed 10 m/s simulations.

At first, we only ran the solar zenith angle 0 degree situation. Figure 28 and Figure 29 show the radiance and percent difference relationships just above the sea surface, for solar zenith angle 0 degrees.

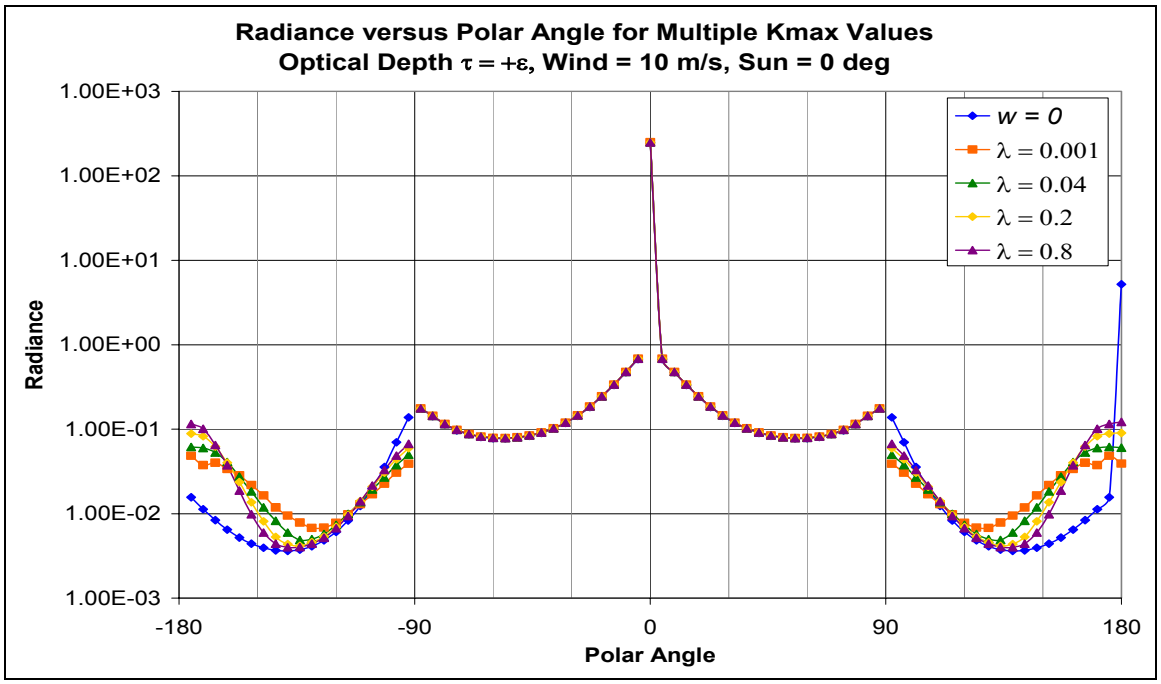

Figure 28 Logarithmic Radiance versus Polar Angle graph for detectors just above the sea surface, and multiple K_{max} values corresponding to cut-off wavelengths 0.001, 0.04, 0.2, and 0.8 meters. Solar zenith angle 0 degrees. Wind speed, *w*, of 0 m/s is included as a comparison.

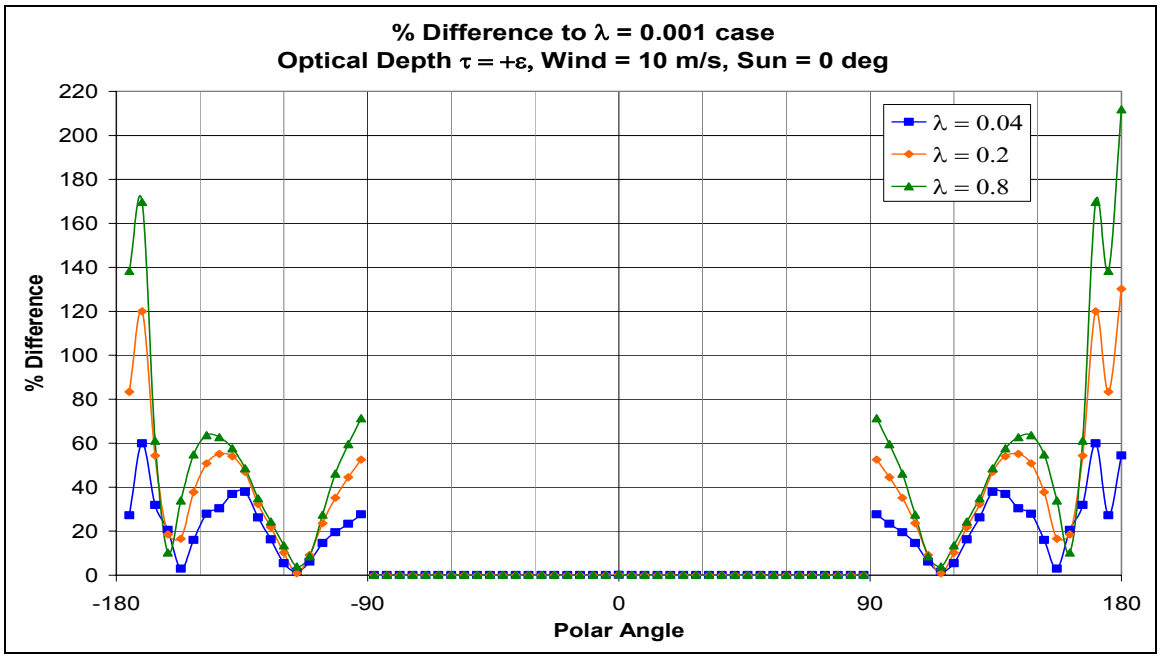

Figure 29 Percent Difference Between Longer Cut-off Wavelengths and the λ = 0.001 Case versus Polar Angle graph for detectors just above the sea surface.

The peak percent difference above the sea surface for wind speed 10 m/s is much greater than that for wind speed 5 m/s. In the 10 m/s case, the differences between corresponding wind speed are greater than in the 5 m/s case. This trend continues with greater optical depth. Figure 30 and Figure 31 show the radiance and percent difference relationships just below the sea surface, for solar zenith angle 0 degrees.

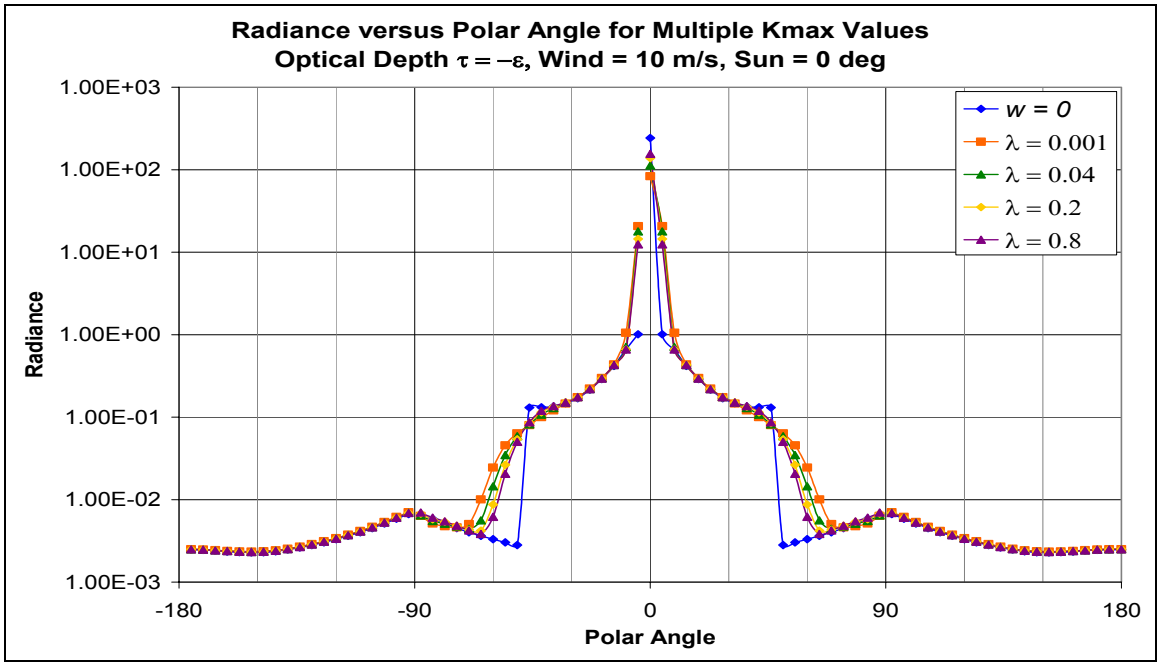

Figure 30 Logarithmic Radiance versus Polar Angle graph for detectors just below the sea surface, and multiple K_{max} values corresponding to cut-off wavelengths 0.001, 0.04, 0.2, and 0.8 meters. Solar zenith angle 0 degrees. Wind speed, *w*, of 0 m/s is included as a comparison.

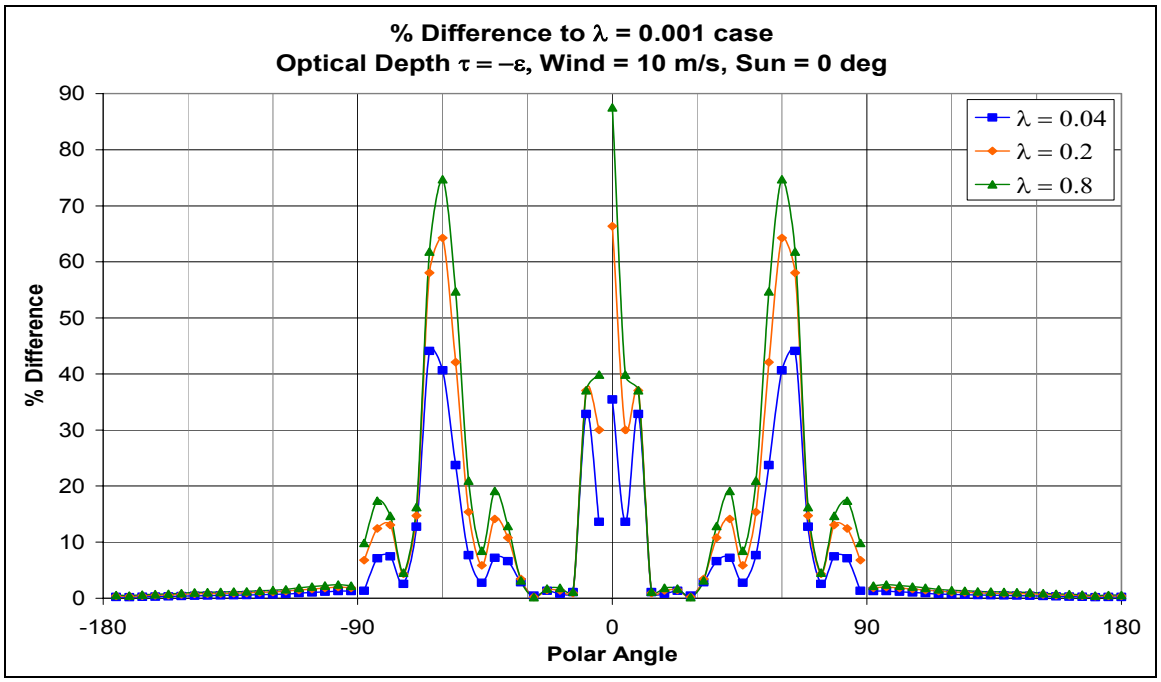

Figure 31 Percent Difference Between Longer Cut-off Wavelengths and the λ = 0.001 Case versus Polar Angle graph for detectors just below the sea surface.

As in the previous two cases, the peak percent difference lies in the diffuse and beam regions. The trend of decreasing peak percent difference with increasing depth is also found in this simulation. Figure 32 and Figure 33 show the radiance and percent difference relationships at optical depth 1 below the sea surface, for solar zenith angle 0 degrees.

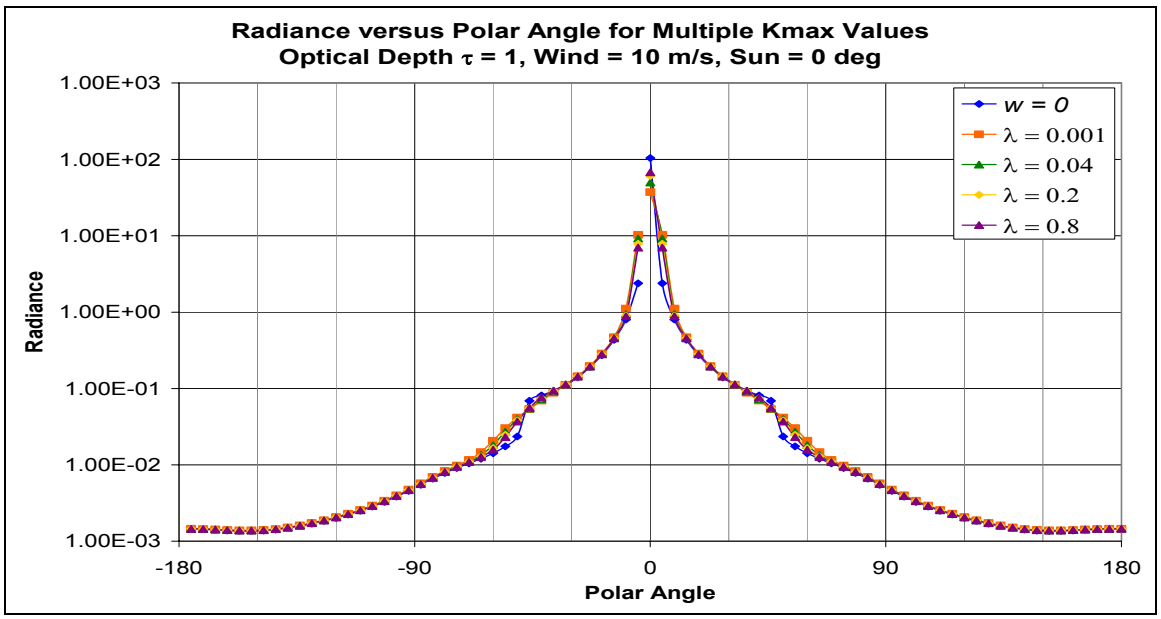

Figure 32 Logarithmic Radiance versus Polar Angle graph for detectors at optical depth 1 below the sea surface, and multiple K_{max} values corresponding to cut-off wavelengths 0.001, 0.04, 0.2, and 0.8 meters. Solar zenith angle 0 degrees. Wind speed, *w*, of 0 m/s is included as a comparison.

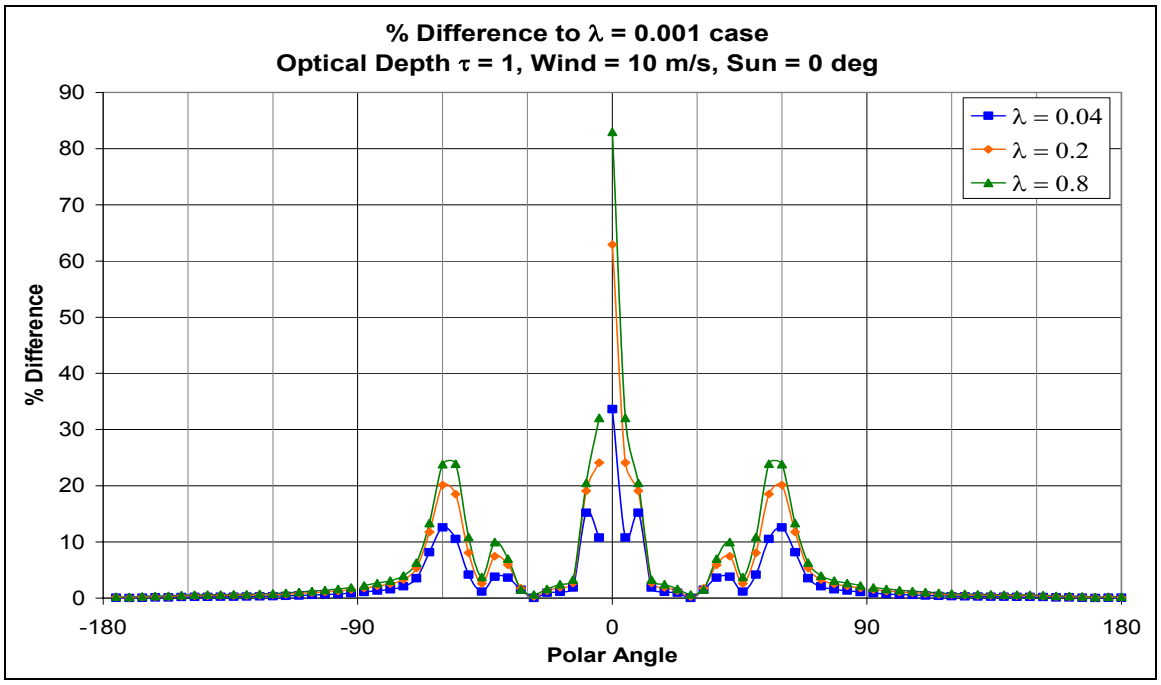

Figure 33 Percent Difference Between Longer Cut-off Wavelengths and the λ = 0.001 Case versus Polar Angle graph for detectors at optical depth 1 below the sea surface.

Figure 34 and Figure 35 show the radiance and percent difference relationships at optical depth 2 below the sea surface, for solar zenith angle 0 degrees.

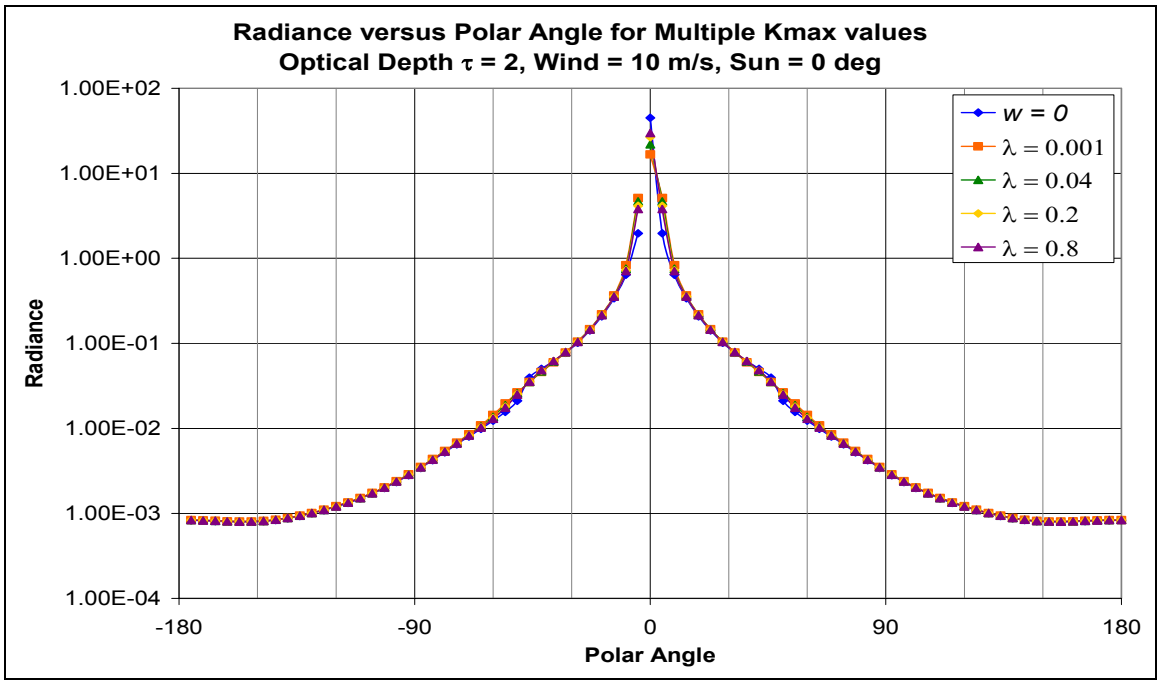

Figure 34 Logarithmic Radiance versus Polar Angle graph for detectors at optical depth 2 below the sea surface, and multiple K_{max} values corresponding to cut-off wavelengths 0.001, 0.04, 0.2, and 0.8 meters. Solar zenith angle 0 degrees. Wind speed, *w*, of 0 m/s is included as a comparison.

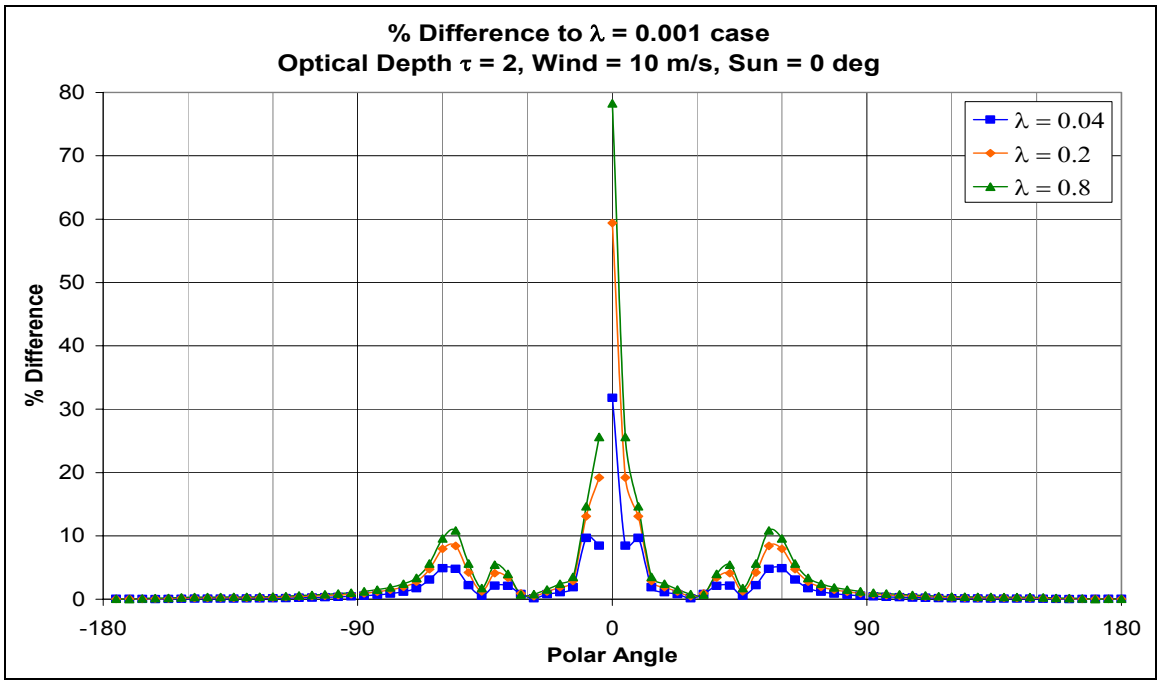

Figure 35 Percent Difference Between Longer Cut-off Wavelengths and the λ = 0.001 Case versus Polar Angle graph for detectors at optical depth 2 below the sea surface.

Figure 36 and Figure 37 show the radiance and percent difference relationships at optical depth 5 below the sea surface, for solar zenith angle 0 degrees.

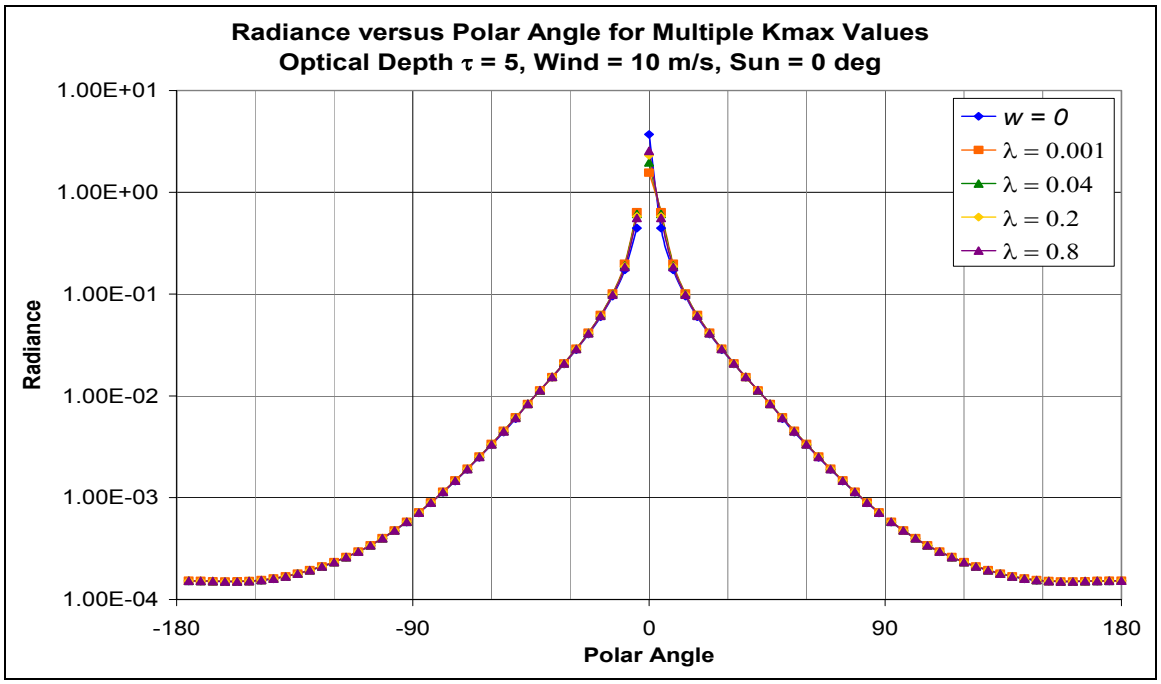

Figure 36 Logarithmic Radiance versus Polar Angle graph for detectors at optical depth 5 below the sea surface, and multiple K_{max} values corresponding to cut-off wavelengths 0.001, 0.04, 0.2, and 0.8 meters. Solar zenith angle 0 degrees. Wind speed, *w*, of 0 m/s is included as a comparison.

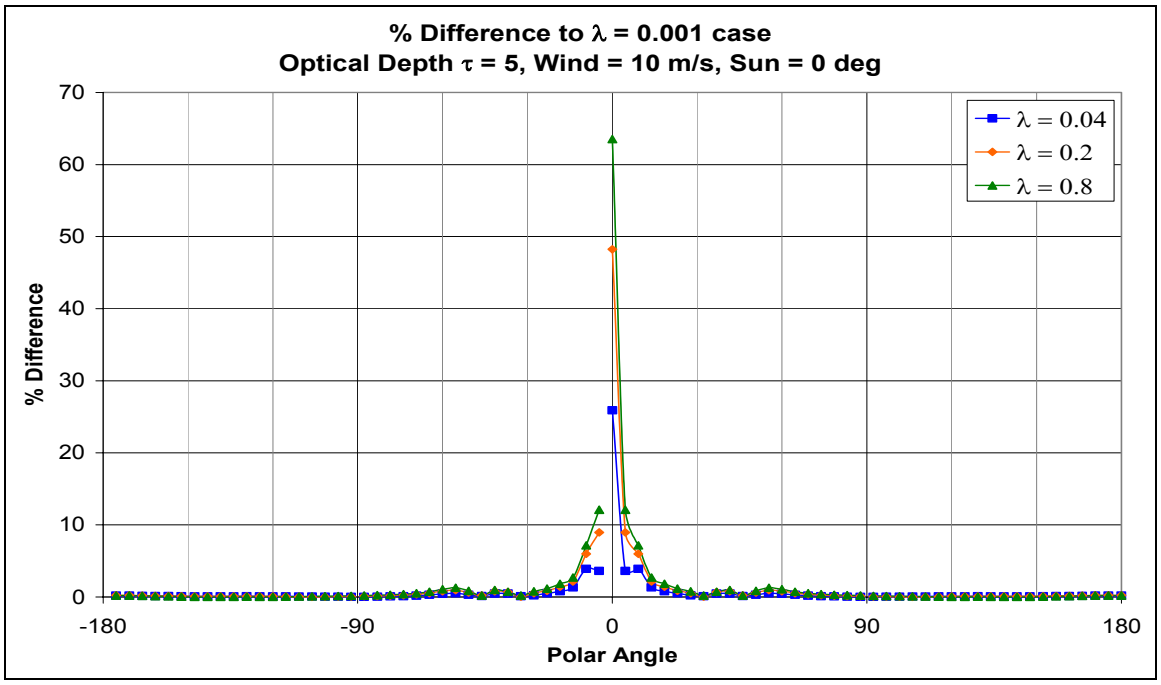

Figure 37 Percent Difference Between Longer Cut-off Wavelengths and the λ = 0.001 Case versus Polar Angle graph for detectors at optical depth 5 below the sea surface.

Figure 38 and Figure 39 show the radiance and percent difference relationships at optical depth 10 below the sea surface, for solar zenith angle 0 degrees.

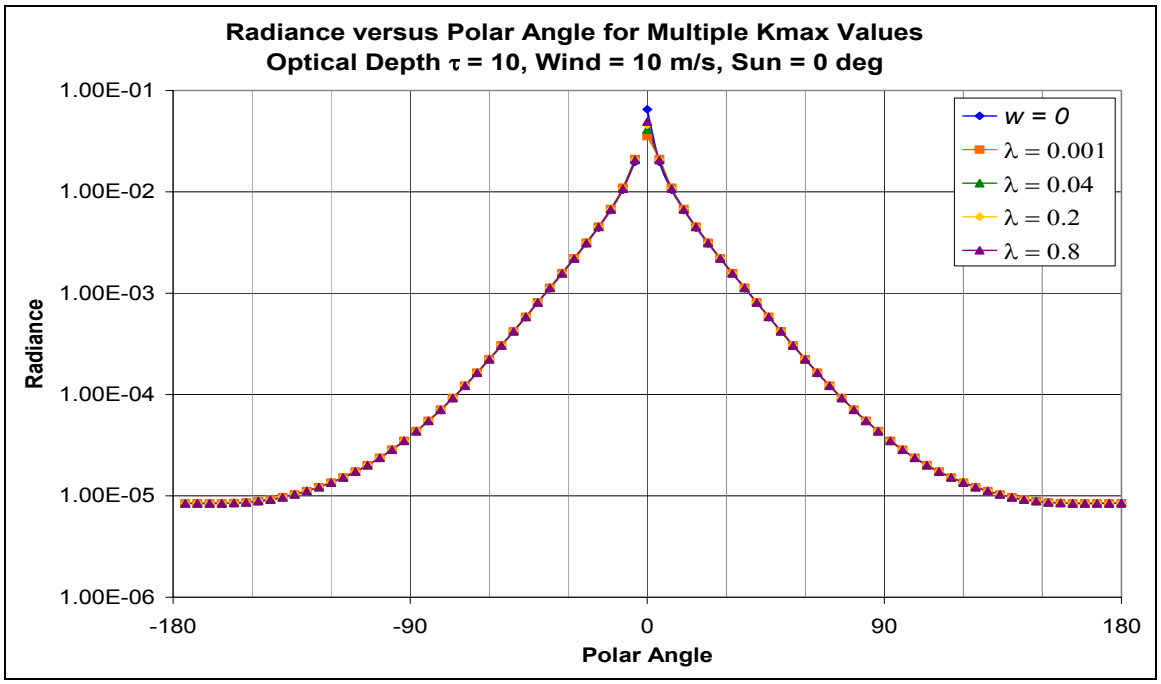

Figure 38 Logarithmic Radiance versus Polar Angle graph for detectors at optical depth 10 below the sea surface, and multiple K_{max} values corresponding to cut-off wavelengths 0.001, 0.04, 0.2, and 0.8 meters. Solar zenith angle 0 degrees. Wind speed, *w*, of 0 m/s is included as a comparison.

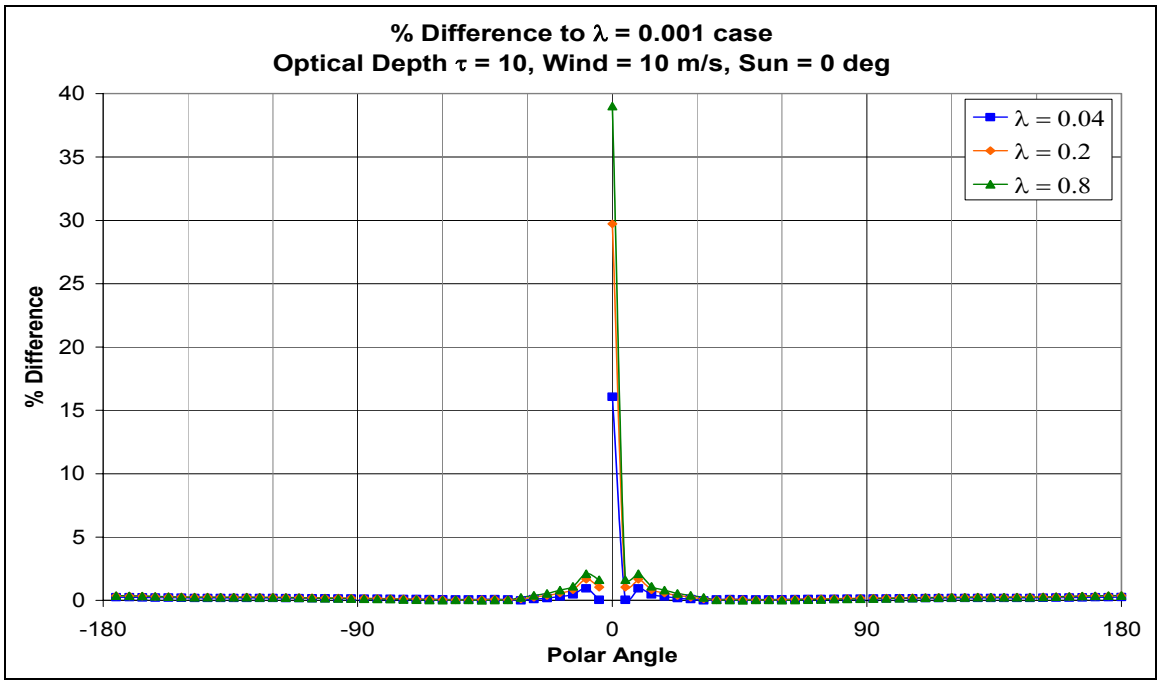

Figure 39 Percent Difference Between Longer Cut-off Wavelengths and the λ = 0.001 Case versus Polar Angle graph for detectors at optical depth 10 below the sea surface.

The data from all optical depths for the wind speed 10 m/s simulation reaffirms all that we have observed in the previous two, wind speed 5 m/s, simulations.

5. Conclusions

As shown above, using the data from three Hydrolight 4.1 simulations, there is a definite and pronounced effect on radiance when the higher frequencies, shorter wavelengths, are truncated out of the root mean square integral.

At all depths, above and below the sea surface, for every situation, the data from the *most* truncated spectrum shows the largest percent difference to the non-truncated spectrum.

At all depths, below the surface, for all wind speed and solar zenith angle situations, there is a peak percent difference to the non-truncated spectrum, in the direction of the solar beam. Also, for all situations, as depth increases, the value of the peak percent difference in the solar beam decreases.

There are also peaks in percent difference found in the diffuse region around -48 degrees and 48 degrees, which is the critical angle for a flat sea surface. However, the value of these peaks decreases much more rapidly with depth than that of the solar beam. In the both of the cases for wind speed 5 m/s, the peaks decrease to small bumps at optical depth $\tau = 5$, and are non-existent at optical depth $\tau = 10$.

In the wind speed 10 m/s case, the peak percent differences in the diffuse region decrease even more rapidly, and are non-existent at optical depth $\tau = 5$. The differences in

corresponding wind speed have a decreasing effect on radiance, with increasing depth, causing the percent differences to decrease, in some manner, at every polar angle.

In the situations with solar zenith angle 0 degrees, there is symmetry in the radiance and also in the percent difference curves. This is not the case for the solar zenith angle 30 degrees situation. At each optical depth, the peak percent difference in the diffuse region around -48 degrees has a higher value than the peak percent difference in region around 48 degrees.

.

References

1. T. Elfouhaily, B. Chapron, K. Katsaros, and D. Vandemark, "A unified directional spectrum for long and short wind-driven waves," J. Geophys. Res. **102**, 15,781-15,796 (1997).
2. C. Cox and W. Munk, "Measurement of the Roughness of the Sea Surface from Photographs of the Sun's Glitter," Journal of the Optical Society of America **44**, 838-850 (1954).
3. T. H. Waterman, "Reviving a neglected celestial underwater polarization compass for aquatic animals," Biol. Rev. **81**, 111-115 (2006).
4. B.Lundgren and N. Hojerslev, "Daylight Measurements in the Sargasso Sea. Results from the 'Dana' expedition, January-April 1966," Kobernhavns Univ. Inst. For Fysisk Oceanografi – Report N. 14 (1971).
5. J. T. Adams, E. Aas, N. Hojerslev, and B. Lundgren, "Comparison of radiance and polarization values observed in the Mediterranean Sea and simulated in a Monte Carlo model," Applied Optics **41**, 2724-2733 (2002).
6. C. D. Mobley, B. Gentili, H. R. Gordon, Z. Jin, G. W. Kattawar, A. Morel, P. Reinersman, K. Stamnes, and R. H. Stavn, "Comparison of numerical models for computing underwater light fields," Applied Optics **32**, 7484-7504 (1993).